ACCSCIENCE PUBLISHING

International Journal of Bioprinting

REVIEW ARTICLE

From cells to organs: Technical challenges of two-photon polymerization in biomedical engineering

Yanzhe Fu[1,2,3,4,5†], Mingming Huang[6†], Jiayong Wei[7], Xiang Ding[5], Bosong Yu[8], Jiebo Li[1,2,3,4,*], Jianmin Han[9*], Lizhen Wang[1,2,3,4*], and Yubo Fan[1,2,3,4*]

[1]Key Laboratory of Biomechanics and Mechanobiology, Ministry of Education, Beihang University, Beijing, China

[2]Key Laboratory of Innovation and Transformation of Advanced Medical Devices, Ministry of Industry and Information Technology, Beihang University, Beijing, China

[3]National Medical Innovation Platform for Industry–Education Integration in Advanced Medical Devices, Beihang University, Beijing, China

[4]School of Biological Science and Medical Engineering, Beihang University, Beijing, China

[5]Center for Medical Metrology, National Institute of Metrology, Beijing, China

[6]Department of Dental Materials, Peking University School and Hospital of Stomatology, Beijing, China

[7]Industrial Science and Engineering Technology Laboratory, Hangzhou International Innovation Institute, Beihang University, Hangzhou, Zhejiang, China

[8]School of Instrumentation and Optoelectronic Engineering, Beihang University, Beijing, China

[9]Department of Prosthetics, Tianjin Medical University School and Hospital of Stomatology, Tianjin, China

[10]Tianjin Key Laboratory of Oral Soft and Hard Tissues Restoration and Regeneration, Tianjin, China

(This article belongs to the *Special Issue*: *Three-Dimensional (3D) Bioprinting for Tissue Engineering and Food Printing*)

Abstract

Nanomanufacturing technology is crucial in advancing sophisticated biomedical devices, biochips, tissue engineering, and advanced biomedical materials. Two-photon polymerization (TPP) offers nanoscale fabrication precision, eliminates the need for masks, and allows the creation of arbitrary three-dimensional structures, providing technical advantages unparalleled by traditional methods. Applying TPP technology in the biomedical field presents new challenges related to materials and systems. Although there has been significant discussion regarding biomaterials, comparatively little attention has been given to the limitations of manufacturing systems for biomedical functional devices. Commercial TPP systems predominantly rely on point-by-point scanning for fabrication, which leads to low throughput. From a biomedical perspective, the goal is to achieve manufacturing precision at the single-cell level while scaling production throughput to the organ level. Advancements in precision and throughput are critical to expanding the applications of TPP in biomedical engineering. This review introduces the fundamental principles of TPP and summarizes recent advancements in TPP applications within tissue engineering, medical devices, and microfluidics. It then delves into the technological progress of TPP in recent years, focusing on aspects such as system design, manufacturing processes, and fabrication principles. The review highlights advancements in areas including the kinetics of light–matter interactions and the development of

[†]These authors contributed equally to this work.

***Corresponding authors:**
Jiebo Li (jiebo39@buaa.edu.cn)

Jianmin Han (hanjm@tmu.edu.cn)

Lizhen Wang (lizhenwang@buaa.edu.cn)

Yubo Fan (yubofan@buaa.edu.cn)

Citation: Fu Y, Huang M, Wei J, *et al.* From cells to organs: Technical challenges of two-photon polymerization in biomedical engineering. *Int J Bioprint*. 2025;11(5):122-153. doi: 10.36922/IJB025280281

Received: July 11, 2025
Revised: August 5, 2025
Accepted: August 13, 2025
Published online: August 20, 2025

cutting-edge techniques such as spatiotemporal focusing. Finally, it discusses future development directions of TPP technology in biomedical applications.

Keywords: Biomedical functional devices; Kinetics; Spatiotemporal focusing; Tissue engineering; Two-photon polymerization

1. Introduction

High-precision manufacturing technology plays a vital role in advancing the biomedical field. Fabricating structures at the micro- and nanoscale facilitates the analysis of interactions between cells and their environment at the single-cell level, enhancing our understanding of various physiological processes under microenvironmental influences.[1] Moreover, developing micro and nanoscale implantable medical devices can minimize trauma to patients, enable more precise imaging and treatment targeting specific disease sites, and improve patient compliance.[2] Additionally, by mimicking the structure of biological tissues and analyzing the macroscopic property changes induced by microstructures, these technologies advance the development of biomimetic materials.[3]

Contemporary micro- and nano-manufacturing technologies include ultraviolet lithography, electron beam lithography, nanoimprint lithography, projection micro stereolithography, and laser direct writing. While ultraviolet and electron beam lithography offer high precision, they face challenges in crafting complex three-dimensional (3D) structures. Nanoimprint lithography excels in precision and efficiency but requires specific molds, which limits its adaptability to unique scenarios. Projection micro stereolithography achieves micrometer-scale precision in 3D structure fabrication, but it has yet to achieve single-cell precision, particularly in hydrogels. Laser direct writing, which requires minimal environmental control, does not need masks, and can create 3D structures, possesses an irreplaceable advantage in fabricating specialized micro and nanoscale structures.

Laser direct writing based on linear absorption can achieve sub-micron precision, yet it is restricted by the diffraction limit, which makes manufacturing features smaller than the wavelength challenging. Two-photon polymerization (TPP), utilizing the nonlinear absorption of materials with femtosecond lasers, can overcome the diffraction limit and significantly enhance structural precision.[4] However, as precision increases, the efficiency of this technique decreases significantly, thereby limiting its further development in the biomedical field.

Numerous excellent reviews have delved into TPP bioprinting, exploring domains including polymers, biodegradable materials, and hydrogels.[5–7] In addition to material-focused discussions, technological advancements play a crucial role in driving the biomedical applications of TPP. This review is prompted by the demand for biomedical applications and aims to provide a comprehensive discussion on the development trends of TPP. As shown in Figure 1, this paper explores TPP, explaining its fundamental principles and outlining its current applications in biomedical engineering, particularly in tissue engineering scaffolds, medical devices, and microfluidic chips. It analyzes the limitations of current mainstream techniques for enhancing the efficiency and precision of TPP and concludes by summarizing the technological advancements and forecasting future trends and potential applications.

2. The principle of two-photon polymerization

TPP is a 3D micro/nano-fabrication technique that employs a femtosecond laser. Femtosecond laser pulses possess an ultrashort duration, on the order of femtoseconds (1 fs = 10^{-15} s), allowing for extremely high peak powers at equivalent average power compared to a continuous laser. The high peak power enables a wide range of physical and chemical processes during material interactions. The nonlinear interactions between femtosecond lasers and materials facilitate the ultra-precise manufacturing of challenging materials and complex micro/nano structures.

In conventional photopolymerization, a single photon absorbed by a dye, initiator, or photosensitizer generates free radicals or cations, thereby triggering monomer polymerization. Conversely, TPP requires simultaneous absorption of two photons to induce the polymerization reaction. The single-photon absorption cross-section is around $\sigma_1=10^{-18}\sim10^{-17}$ cm^2, whereas the two-photon absorption cross-section is approximately $\sigma_2=10^{-50}\sim10^{-46}$ cm^4, indicating that polymerization can occur solely in regions with sufficiently high light intensity.[8] Figure 2A illustrates the single-photon absorption process, in which fluorescence is excited throughout the dye region. In contrast, the two-photon absorption process confines fluorescence signals to the laser focus, where the photon density is sufficiently high. This selective excitation of

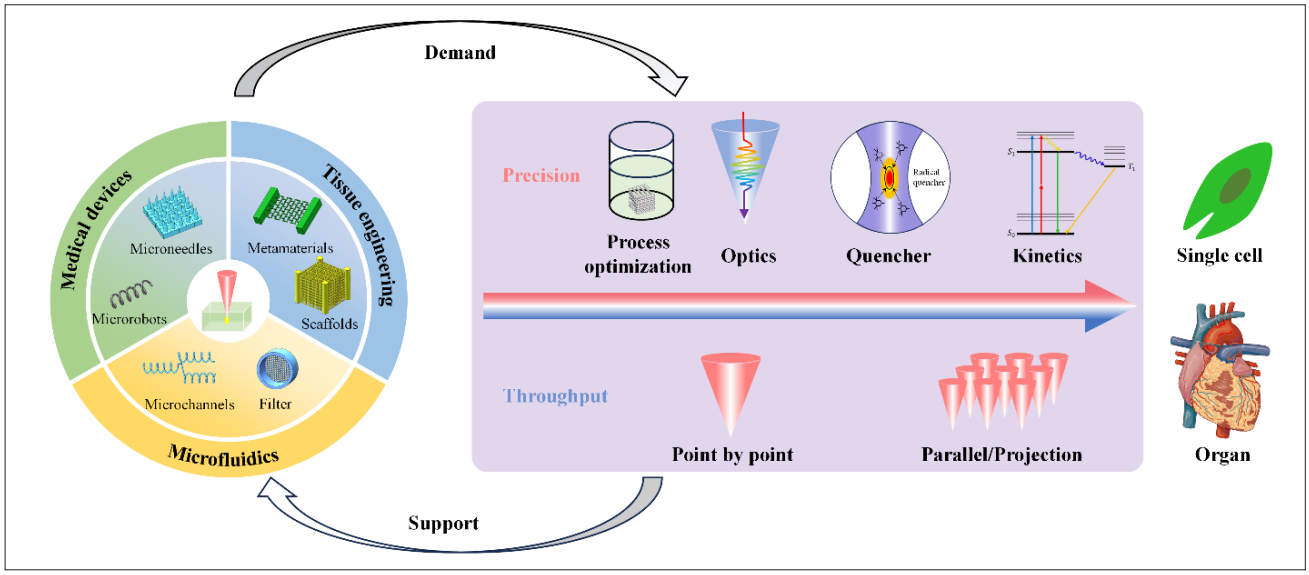

Figure 1. The relationship between biomedical applications and the evolutionary trends of two-photon polymerization. The heart image was adapted from Servier Medical Art.

chemical reactions via two-photon absorption within a transparent medium enables the fabrication of authentic 3D structures. The interaction between light and matter during 3D printing is illustrated in Figure 2B.[9] In the ground-state initiator molecule (S_0), electrons in the highest occupied molecular orbital typically exist as a pair with opposite spins. Upon photon absorption, one of these electrons acquires energy and transitions to the lowest unoccupied molecular orbital, forming an excited singlet state (S_1). Variations in the power of femtosecond laser pulses and photoresist systems yield distinct nonlinear interactions.[10,11] The excited initiator molecules may return to S_0 via spontaneous or stimulated fluorescence, undergo excited-state absorption to higher energy levels,

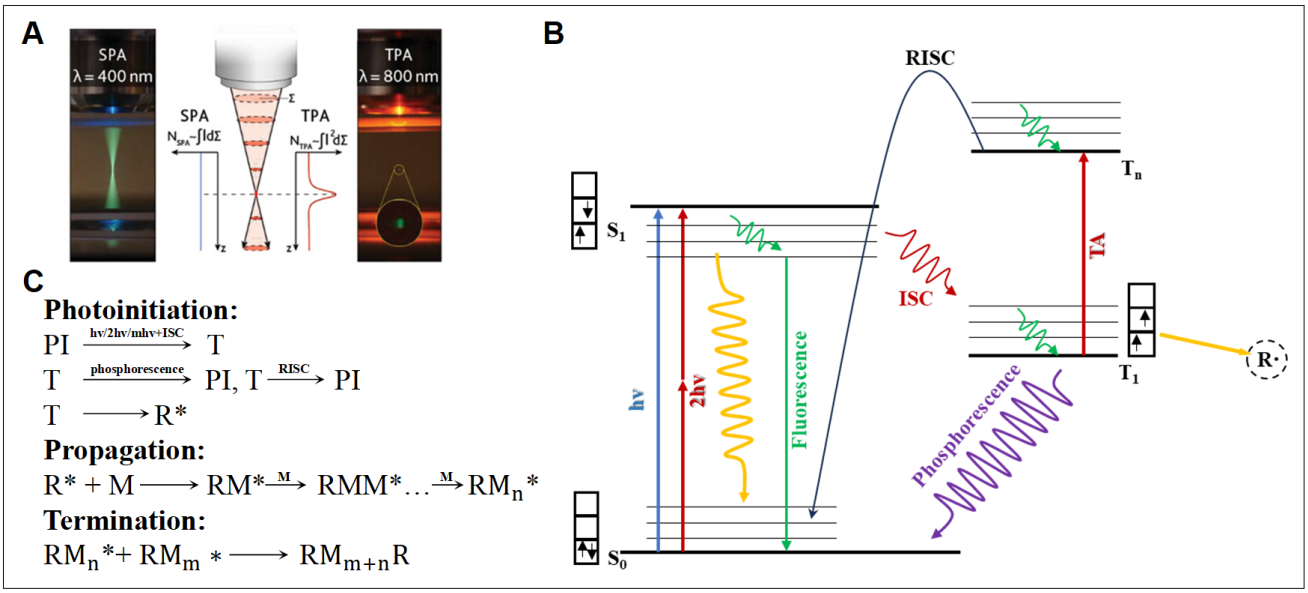

Figure 2. Schematic illustration of the principle of TPP. (A) The differences between SPA and TPA. Adapted with permission from ref.[12] Copyright © 2025 Wiley. (B) Energy level diagram of light–matter interaction during the three-dimensional printing process. (C) The process of the TPP reaction, where PI is the photoinitiator, RM is the monomer radical, *M* is a monomer, and M_n is a polymeric chain of *n* monomers. Abbreviations: ISC, intersystem crossing; RISC, reverse intersystem crossing; SPA, single-photon absorption; TPP, two-photon polymerization; TPA, two-photon absorption.

or transition to a triplet state (T_1) through intersystem crossing (ISC). During the ISC from S_1 to T_1, the spin of the excited electron undergoes inversion. This spin inversion leads to the excited electron's spin aligning parallel to its paired ground-state electron, yielding a parallel spin configuration. Molecules in the triplet state can return to the ground state through phosphorescence, undergo triplet-state absorption to higher energy levels followed by reverse ISC, or directly generate free radicals (R*). Furthermore, triplet-state absorption may result in the formation of higher-level free radicals.

The TPP process consists of three primary steps: chain initiation, chain growth, and chain termination, as illustrated in Figure 2C. Photoinitiator molecules in the ground state (PI) within the photoresist generate free radicals (R*) through a series of dynamic processes. These free radicals then react with monomers or oligomers (M), resulting in monomer radicals (RM*). These radicals propagate via a chain reaction to form (RMn*). The chain reaction is terminated when two monomer radicals meet.

In 1997, Maruo *et al.*[13] pioneered the application of TPP for the fabrication of 3D structures, successfully creating helical architectures in three dimensions.[13] In 2001, the research team employed a femtosecond laser to fabricate a "micro-bull" measuring 10 μm in length and 7 μm in height, thereby establishing a seminal milestone within the domain of TPP. This work represented a groundbreaking advancement by surpassing the optical diffraction limit, achieving a processing resolution of 120 nm, significantly exceeding the diffraction limit of 460 nm, thereby indicating the progressive maturation of TPP.[4]

3. The application of two-photon polymerization in biomedical engineering

TPP provides new possibilities for biomedical engineering research and applications, including tissue engineering, medical devices, and biochips. In biomedical applications, the biocompatibility of materials must also be taken into consideration. Commonly used photoinitiators are typically lipophilic, whereas biocompatible materials such as hydrogels require water-soluble photoinitiators, posing significant challenges for the application of TPP. Some of these aspects have been addressed in previous reviews[5] and will not be elaborated further in this paper.

3.1. Tissue engineering

In 1993, Robert Langer[14] defined tissue engineering as a modern science that is an interdisciplinary field that applies the principles of life sciences and engineering to the development of biological substitutes that restore, maintain, or improve tissue function.[14]. In the past 30 years, tissue engineering has achieved rapid progress. It plays a significant role in healing bone and cartilage defects, skin burns, nervous system injuries, corneal replacement, and cosmetic surgery. Tissue engineering technology generates the organization by adding suitable cells and materials to specific scaffolds. Most cells other than blood cells exist within the extracellular matrix (ECM). Ideally, for a specific organization, the best 3D scaffolds are its original ECM. However, the native ECM has diverse functions, complex compositions, and dynamic changes; to build such an environment *in vitro* is extremely challenging.[15] When fabricating scaffolds, even if the functions of ECM cannot be completely mimicked, it is necessary to mimic the functions of ECM, including good biocompatibility, bioactivity, and mechanical properties. The ideal 3D scaffold should possess a porous structure, network connection, and uniform pore size to facilitate cell migration and invasion.

At present, various techniques have been used to fabricate tissue engineering scaffolds, such as spinning,[16] thermally induced phase separation,[17] solvent casting/particle leaching,[18] and membrane laminating.[19] However, these techniques fail to precisely control the structure, pore size, and network of scaffolds. With the advent of 3D printing, it has become possible to fabricate scaffolds with controllable structures and sizes.[20] Compared to other methods, optical printing not only has higher precision, but can also be applied to different materials, including polymers, metals, and ceramics, and can meet the requirements of different application scenarios, which has been widely concerned. Currently, primary optical printing methods in tissue scaffolds fabrication are TPP, stereolithography apparatus, selective laser melting, and light-curing material jetting/extrusion.[21,22] The size of a typical cell is generally within the micron range, and to ensure that interactions between cells and their microenvironment are not compromised, the scale of the scaffold structure must closely match the cell size. This necessitates manufacturing precision within the range of 0.1–10 μm. Among all the above 3D fabrication technologies, only TPP can achieve the fabricated feature size below 1 μm; therefore, TPP is of great value for tissue engineering and regenerative medicine.[20,23,24] At present, engineering scaffolds manufactured based on TPP have been used in the culture of many cell systems.

In 2007, Ovsianikov and coworkers[25] successfully created 3D scaffolds with the TPP technique using commercially available photoresist SU8 and ORMOCER®, demonstrating their ability to support cell growth.[25] In 2010, Klein *et al.*[26] utilized the 3D scaffold fabricated by TPP to analyze the stress change during cell growth, demonstrated that the beam in

contact with the cell was bent and stretched during a single contraction cycle of the cardiomyocyte, and tested its deflection (Figure 3A).[26] In 2011, this group combined TPP with composite materials to obtain two-component 3D scaffolds with distinct mechanical and protein-binding properties, achieving full control over the formation of cell adhesion sites and cell shape in three dimensions (Figure 3B).[27] In 2017, Ricci *et al.*[28] fabricated tightly packed tissue engineering scaffolds and demonstrated the culture results of human bone marrow mesenchymal stem cells with 88% surface coverage.[28] In the same year, Turunen *et al.*[29] fabricated a tubular microtower-based 3D platform featuring intraluminal guidance cues and wall openings via TPP for culturing human pluripotent stem cell-derived neuronal cells.[29] Tissue scaffolds fabricated by TPP can influence cell culture not only through structural design but also by dynamically altering the mechanical properties of the microenvironment. In 2017, Lemma *et al.*[30] exploited an innovative polymeric scaffold based on TPP, featuring cage-like structures and cylindric stent-like micro-scaffolds fabricated with varying Young's moduli and stiffness gradients. These scaffolds allowed precise control of 3D microenvironmental stiffness to study cancer cell invasiveness and analyze how external mechanical properties influence cellular behavior (Figure 3C).[30] In 2018, Tudor *et al.*[31] achieved the creation of soft, stimulus-responsive 3D structures using crosslinked poly(ionic liquid)s through TPP. These structures exhibit properties such as swelling, temperature response (known as the four-dimensional effect), and programmed movement.[31] Marino *et al.*[32] innovatively fabricated a 1:1 real-scale biomimetic and biohybrid blood–brain barrier model by TPP. The system co-cultured endothelial and glioblastoma cells on biomimetic microtubes inspired by the brain capillaries, demonstrating mature tight junctions. Combined with mathematical optimization of fluid

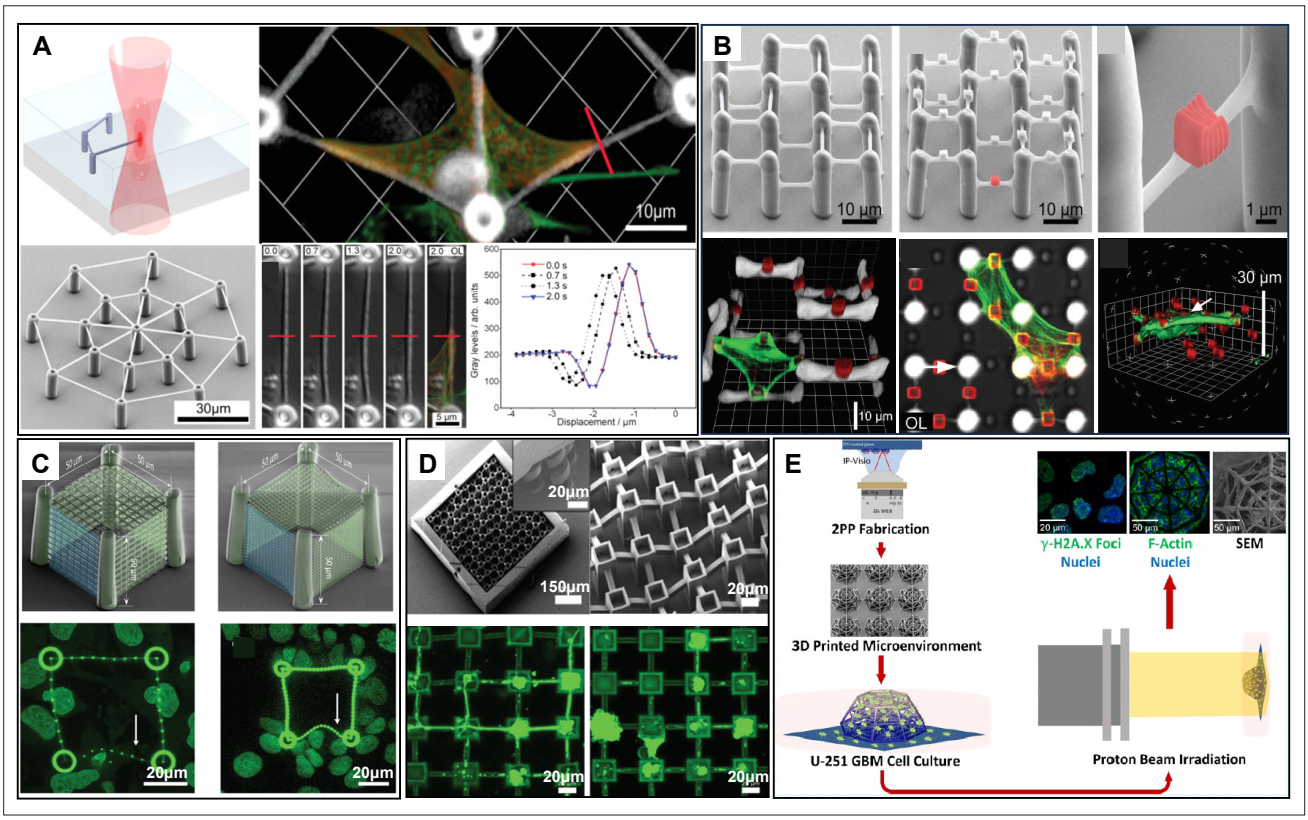

Figure 3. Tissue engineering scaffolds fabricated using two-photon polymerization. (A) Three-dimensional (3D) scaffolds utilized to analyze the stress change during a single contraction cycle of the cardiomyocyte. Scale bars: 5, 10, and 30 μm. Reproduced with permission from Klein *et al.*[26] Copyright © 2010, Wiley. (B) Two-component 3D scaffolds with distinct mechanical and protein-binding properties. Scale bars: 1, 10, and 30 μm. Reproduced with permission from Klein *et al.*[27] Copyright © 2011, Wiley. (C) 3D scaffolds with different Young's modulus and stiffness gradients to study cancer cell invasiveness. Scale bar: 20 μm. Reproduced with permission from Lemma *et al.*[30] Copyright © 2017, Wiley. (D) 3D neuronal scaffolds to culture neurons *in vitro*. Scale bars: 20 and 150 μm. Reproduced with permission from Fendler *et al.*[33] Copyright © 2019, Wiley. (E) Research on assessing the effects of proton beam therapy on 3D glioblastoma cell networks. Reproduced with permission from Akolawala *et al.*[34]

dynamics, this system offers a referenceable *in vitro* model for investigating the delivery of nanomaterial/drug across the blood–brain barrier.[32] Given that low-density neuronal cultures *in vitro* are useful for studying neurons at the cellular level, in 2019, researchers used direct laser writing via TPP to fabricate tailor-made 3D culturing substrates. These substrates consisted of pillars with different heights connected through freestanding microtubes with quadratic cross sections (Figure 3D).[33] The truly 3D neuronal networks built in the work combined site-specific chemical-guiding adhesion with topological limitation of potential neurite growth paths to determine predefined pathways as well as guidance paths for controlled axon and dendrite outgrowth. In 2022, Akolawala *et al.*[34] designed 3D scaffolds inspired by the geometry of brain blood vessels to be cultured with U-251 glioblastoma cells and assess their response to proton radiation (Figure 3E).[34] In 2022, Rengaraj *et al.*[35] combined a microscale 3D scaffold to engineer a microscale niche for pancreatic tumor cells fabricated via TPP with a bioactive layer-by-layer film coating. The functionalized scaffold successfully supported 3D tumor-like tissue culture for up to 20 days and revealed significant context-specific cell responses, confirming its potential to simulate the early microenvironment of metastasis and provide a controllable *in vitro* model to study pancreatic cancer mechanisms and drug screening.[35] In 2022, Costa *et al.*[36] optimized 3D woodpile microscaffolds from different photosensitive polymers (IP-S and SZ2080) and hydrogel (PEGDA 700) using TPP and coated them with fibronectin to investigate the behavior of bone marrow mesenchymal stem cells. These scaffolds maintained stemness and supported co-culture with HeLa cells, offering a novel biomimetic platform for modeling bone marrow niches, studying hematological disorders (e.g., leukemia), and advancing drug screening applications.[36]

Currently, tissue engineering scaffolds manufactured using TPP have been successfully applied to various cell lines, including neurons derived from human induced pluripotent stem cells, pancreatic cell lines, and bone marrow mesenchymal stem cells. In tissue engineering, the development of TPP technology has shown a trend of shifting from structure-oriented to function-oriented approaches. Early studies primarily focused on constructing precise 3D cellular microenvironments to enable passive cell growth. With continuous advancements in materials science and manufacturing technologies, current research has begun regulating cell morphology and exploring the impact of microenvironment on cellular behavior. However, during this developmental process, the throughput limitations of TPP manufacturing have constrained the ability to construct highly complex microenvironments. Additionally, beyond existing polymer materials, developing relatively soft hydrogel materials that better facilitate cell adhesion, extension, and growth imposes higher requirements on the light–matter interaction in TPP. If manufacturing throughput can be effectively improved, it could potentially extend single-cell scale regulation capabilities to organ-level applications. Notably, some parallel manufacturing technologies have already provided preliminary implementation pathways for this vision. The deep integration of micro/nano manufacturing techniques with biological 3D printing technology holds promise for catalyzing entirely new paradigms in tissue engineering manufacturing.

3.2. Medical devices

TPP has unlocked new possibilities for medical device fabrication, enabling the creation of micro and nanoscale devices that facilitate minimally invasive, precision medicine—such as microneedles, endoscopes, and micro/nano robots.

Advances in genetic engineering and proteomics technology have introduced protein- and nucleic acid-based therapies for cancer and other chronic diseases. However, many of the pharmacologic agents are not suitable for oral or transdermal use, as the liver, kidney, and other organs may metabolize them. Therefore, intravenous injection can improve drug absorption in the human body, while the traditional hypodermic needles are less suitable for extended delivery, causing pain and trauma at the injection site and requiring professional administration. Microneedles, as a minimally invasive drug delivery method, possess a needle size of 300–400 μm, which can avoid pain to the patient and reduce bruising to the injection site.[37] Hollow microneedles can enable slow release of medicine over a longer period through diffusion- or pressure-driven transport. Compared to solitary needles, arrays of microneedles can provide injection or extraction over a wider area and at higher rates. In 2007, Ovsianikov *et al.*[38] created 3D hollow microneedle arrays with complex geometries using TPP, which demonstrated the applicability of TPP on large-area fabrication of microneedles and the possibility of using TPP for portable medical devices.[38] In addition to drug delivery, microneedles also hold great promise for vaccine injection. The use of microneedles can avoid medical waste generated by traditional subcutaneous and intramuscular injections and reduce the risk of infection caused by reusing syringes.[39] In 2017, Rad *et al.*[40] combined hollow microneedles with open microfluidic channels to fabricate novel microneedle arrays for subcutaneous fluid sampling and drug delivery,

demonstrating that TPP is more flexible in fabricating micro/nano devices (Figure 4A).[40] In 2020, Balmert *et al.*[41] used TPP to produce master molds of microneedle arrays to generate dissolving undercut microneedle arrays for multicomponent cutaneous vaccination, and showed that this drug delivery technology can elicit potent antigen-specific cellular and humoral immune responses through the skin.[41]

Endoscopes can provide diagnostic images of hollow organs at high resolution to assist clinicians in diagnosing and intervening. However, commonly used endoscopes have difficulty imaging small luminal or delicate organs due to the limitations of the traditional fabrication method of endoscopes. In 2020, researchers used TPP to 3D print 125-μm-diameter micro-optics directly onto a single-mode optical fiber (Figure 4B).[42] This is by far the smallest freeform 3D imaging probe and the smallest aberration-corrected intravascular probe reported, with a diameter of 0.457 mm including the catheter sheath, and is able to image atherosclerotic human and mouse arteries.

Moreover, TPP can be applied to create micro/nanorobots for drug delivery, thrombolytic procedures, and assisted reproduction.[43,44] Unlike traditional robots, micro/nanorobots are limited by their minute size, which restricts the integration of complex computational, actuation, sensing, functional, and communication units. Instead, their motion relies predominantly on energy conversion mechanisms and interactions within their microenvironment.[45] The propulsion modes of micro/nanorobots include ultrasonic, chemical, and magnetic propulsion modes.[46–49] Among the various propulsion methods, magnetic field actuation has been extensively employed due to its non-contact operation, safety profile, and precise controllability. Poor sperm motility is one of the main causes of male infertility.[50] In 2015, Medina-Sanchez *et al.*[51] fabricated polymer microhelices using TPP with soft-magnetic nickel–titanium bilayer coatings, which

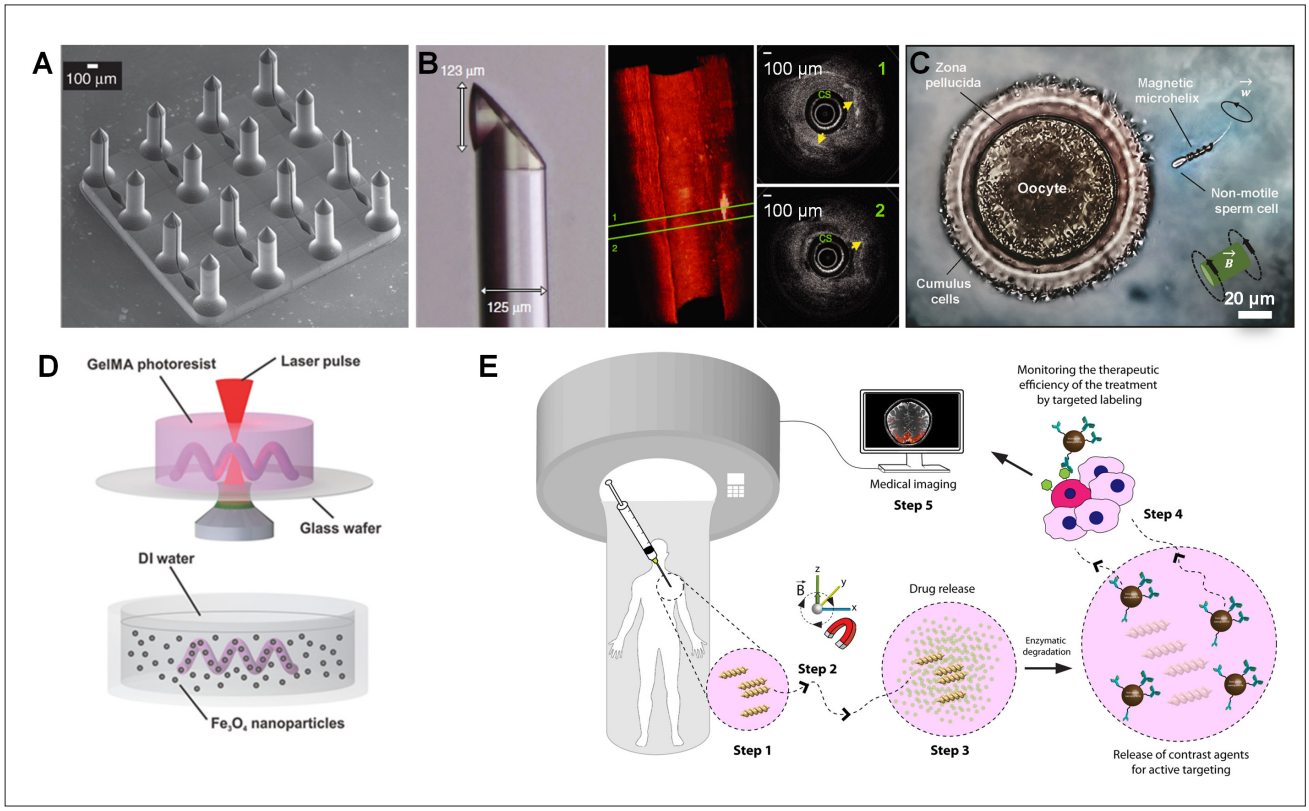

Figure 4. Implantable and interventional medical devices fabricated using two-photon polymerization. (A) Hollow microneedles with open microfluidic channels. Scale bar: 100 μm. Reproduced with permission from Rad *et al.*[40] (B) Micro-optics directly printed onto the single-mode optical fiber. Scale bars: 100 μm. Reproduced with permission from Li *et al.*[42] (C) Sperm carrying micromotors assisted fertilization. Scale bar: 20 μm. Reproduced with permission from Medina-Sanchez *et al.*[51] Copyright © 2016, American Chemical Society. (D) Enzymatically biodegradable soft helical microswimmers. Reproduced with permission from Wang *et al.*[53] Copyright © 2018, Wiley. (E) Biodegradable microswimmer for drug delivery and release. Reproduced with permission from Ceylan *et al.*[54]

showed controllable 3D motion (Figure 4C).[51] Through the rotating magnetic fields generated by Helmholtz coils, microhelices can capture, transport, and release single live sperm cells under physiological conditions. Moreover, sperm cells can be successfully delivered to the oocyte cell wall, which presents the potential of this novel technique toward assisted reproduction. In 2023, Fan *et al.*[52] developed a magnetic fiber robot with integrated terminal functionality, offering a flexible and innovative solution for integrating and assembling distal functional components. This development has considerable potential to advance the miniaturization and functional capabilities of interventional medical robots.[52] Beyond structural design, biocompatibility represents a fundamental consideration for micro/nanorobots. In 2018, Wang *et al.*[53] utilized P2CK as an initiator to fabricate biodegradable micro/nanorobots from gelatin methacryloyl-based materials (Figure 4D).[53] In 2019, Ceylan *et al.*[54] demonstrated precise drug delivery via the controlled degradation of biodegradable microrobots (Figure 4E).[54]

3.3. Microfluidics

Beyond direct fabrication of 3D microfluidic structures, TPP can be applied for the realization of microscale 3D structures printed inside the microchannels, including the nozzle, mixer, filter, and capillary pump, which can expand the diversity and flexibility of microfluidic chips.[55–57]

The number of circulating tumor cells is closely correlated with the lethal potential of the tumor. In 2019, Jiménez-Zenteno *et al.*[57] created a 3D stealthy intravascular microdevice with the aid of TPP, engineered as a hollow circular cylinder with a holey membrane at the downstream end-wall, adapted to the physical capture of circulating tumor cells in the venous blood flow *in vivo*.[57] Biosensors can be fabricated through processing micro/nanoscale 3D structures in the microchannels. In 2020, Lao *et al.*[58] exploited the tendency of delicate micro/nanostructures to collapse during solvent development due to existing capillary forces. They manufactured 3D nanogap-enabled plasmonic structures by combining supercritical drying, noble metal coating, and switchable capillary-force-driven self-assembly of TPP-fabricated micropillars.[58] The nanogap-enabled microfluidic device integrated in microchannels, together with the electromagnetic enhancement, showed great potential for surface-enhanced Raman spectroscopy sensing research. Poorly soluble drugs struggle to elicit effects through oral or parenteral administration, but using lipid nanoparticles as a carrier enabled the drugs to achieve sufficient bioavailability. Microfluidic systems can effectively control the particle size distribution and mixing scheme of nanoparticles. However, there is a risk of particle-containing fluids deposition on the surface of microchannels, which limits the repeatability and stability of long-term continuous processing during practical use. In 2021, Erfle *et al.*[59] created a coaxial lamination mixer using TPP with a unique 3D design to address challenges in the manufacturing process of drug nanoparticles, which can eliminate contact of the organic phase with the channel walls, avoid particle deposition, mix organic and aqueous phases efficiently, and reduce

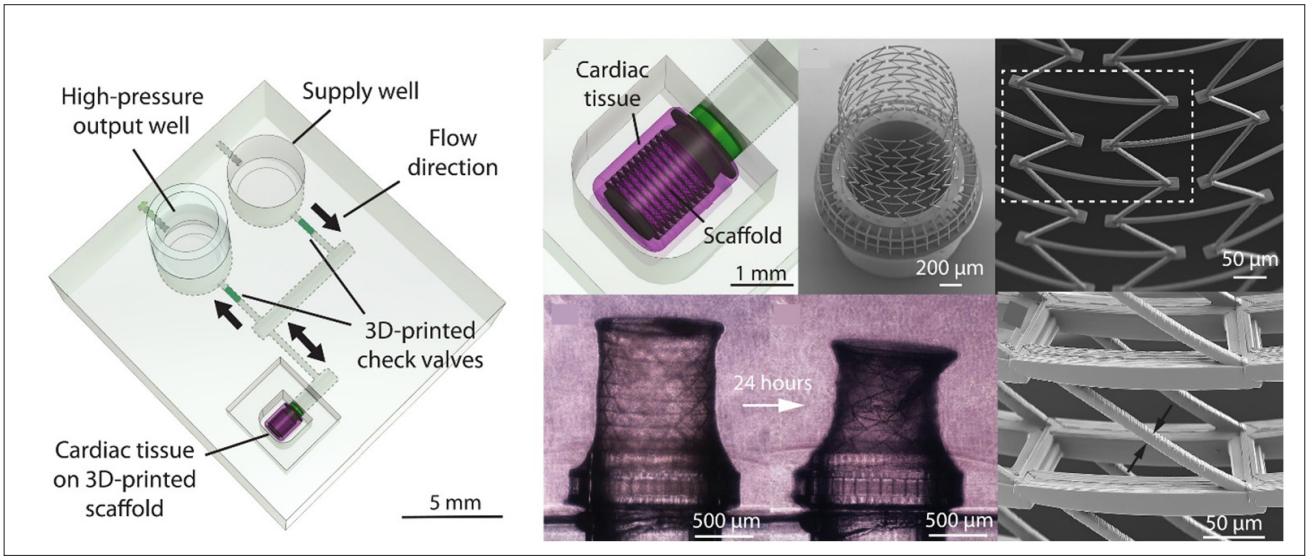

Figure 5. Heart-on-chip system via two-photon polymerization. Scale bars: 1 mm, 5 mm, 50 µm, 100 µm, and 500 µm. Reproduced with permission from Michas *et al.*[60] Copyright © 2022, AAAS Wiley. Abbreviation: 3D, three-dimensional.

fouling, proving the feasibility of this approach in high-throughput monodisperse drug carrier nanoparticles production.[59] In 2022, Michas *et al.*[60] developed a novel heart-on-chip system via TPP (Figure 5). The platform utilized a nanoscale metamaterial scaffold to guide human induced pluripotent stem cells-derived cardiomyocytes into contractile ventricular chambers, integrated with fabricated microfluidic valves for unidirectional flow, achieving the first complete pressure-volume loop *in vitro*. This work overcomes limitations in constructing functionally ordered microstructures for organ chips, providing a vital tool for cardiac biomechanics, drug screening, and disease modeling.[60]

TPP serves as a powerful tool in the biomedical field; however, its manufacturing throughput limits its further development. Precision and efficiency are mutually constrained because the size of a single voxel in TPP is approximately 200 nm, resulting in extremely low efficiency when manufacturing large-scale devices. Assuming a scanning speed of 5 mm/s, fabricating a 1 mm^2 area would take 1×10^3 s. For a 1 mm^3 area with an axial dimension of 500 nm and no voxel overlap, this process would require 2×10^6 s, or approximately 23 days. Moreover, the need to maintain the femtosecond laser in a stable working condition, regulate water content in materials, or preserve cell viability throughout this process imposes significant environmental demands. Therefore, manufacturing efficiency in TPP represents a significant limitation to its further development in the biomedical field. Furthermore, enhancing the precision of TPP could significantly facilitate the observation and study of cellular processes at the single-cell level. Optimizing TPP in terms of precision and efficiency assists in the fabrication of multiscale, hierarchically organized biological structures, which have significant implications for the biomedical field. Researchers have conducted extensive studies to improve the throughput and precision of TPP.

4. Two-photon polymerization throughput enhancement

4.1. Single-focus serial scanning

As illustrated in Figure 6, the mainstream writing methods currently include point-by-point scanning using a translation stage or piezoelectric stage, as well as scanning with a galvo mirror. Additionally, resonant mirrors combined with rapid shutters (such as Pockels cells) are also employed for scanning. During the construction of optical pathways, relay lens groups are carefully selected and configured to achieve the desired spot size and field of view. These approaches can be further categorized into raster scanning and vector scanning.[12]

Manufacturing via TPP typically employs stepper motors or piezoelectric stages to enable precise sample movement. However, due to the inherent inertia of these stages, they are restricted to scanning speeds ranging roughly from 0.1 to 30 mm/s.[61] The use of galvanometer scanners can increase these speeds to several tens or hundreds of millimeter per second; however, this is still insufficient to meet the efficiency requirements for the mass production of most devices. With the advent of novel scanning technologies, researchers have utilized commercial resonant galvanometer mirrors, achieving scanning speeds of up to 8 kHz and an extraordinary 8000

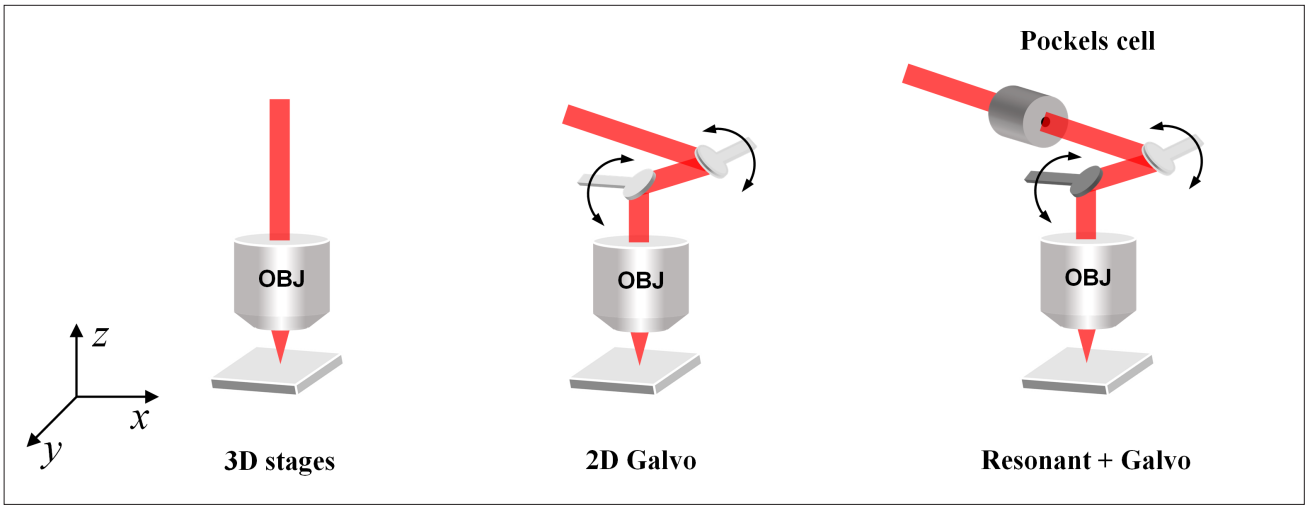

Figure 6. Common scanning methods in two-photon polymerization systems. Created by the authors with Microsoft PowerPoint. Abbreviations: 2D, two-dimensional; 3D, three-dimensional; OBJ, objective.

mm/s, representing the fastest processing throughput for serial scanning known to date.[61] Resonant mirrors, with their high-frequency operation, enable even faster scanning speeds, requiring integration with high-speed shutters to control energy modulation, thereby achieving a raster scanning effect.

4.2. Parallel fabrication

4.2.1. Static multi-foci or light field

To enhance efficiency, optical devices can be employed to generate multiple foci, enabling high-speed fabrication when combined with the scanning method described in Figure 6.

The scanning speed of serial methods is often constrained by the capabilities of scanning devices, whereas parallel devices such as micro lens array (MLA), diffractive optical elements (DOE), and meta-lens facilitate high-efficiency, multi-focus parallel processing, thereby offering the potential for significantly enhanced processing throughput.[62–65] In 2005, Kato's team[66] first introduced a parallel multi-focus printing method using MLA with 41×41 lenses in a 10×10 mm^2 area, achieving simultaneous printing of over 200 points.[66] However, combining the microlens array with a galvanometer to increase manufacturing speed inevitably resulted in aberrations from large-angle incident light.[67] In 2007, Dong *et al.*[68] utilized DOE and a galvanometer to fabricate complex 3D structures, significantly enhancing manufacturing efficiency. Nonetheless, the dispersion and pulse broadening introduced by the optical components reduced the efficiency of two-photon absorption. There is a contradictory relationship between focus size, energy, distribution uniformity, and the number of focal points—more focal points result in lower focus energy, larger laser spots, poorer uniformity, and reduced resolution in direct writing. In 2020, Hahn *et al.*[69] proposed a rapid multi-focus 3D printing method using an acousto-optic modulator instead of a shutter and employing prisms and dispersion-compensating prisms to offset pulse broadening caused by optical components, ensuring the efficiency of two-photon absorption and achieving a printing rate of over 10 million voxels per second.[69] In 2024, the team combined DOE and MLA to optimize dispersion and uniformity, achieving a manufacturing speed of over 10^8 voxels per second (Figure 7).[70]

TPP is fundamentally a photochemical process wherein the spatial distribution of light dictates the polymerization. Compared to point-by-point scanning, light field modulation techniques offer additional dimensions of control for TPP. In 2006, Ježek *et al.*[71] utilized conical lenses to generate Bessel beams, thereby achieving rapid printing of hollow cylindrical structures.[71] In 2012, researchers in Lithuania analyzed the differences among laser direct writing, vortex light, and holographic lithography for fabricating microtubes. Compared to laser direct writing, holographic lithography increased efficiency four hundredfold, and vortex light five hundredfold.[72] In 2014, the team from the University of Science and Technology of China rapidly fabricated arrays of cylindrical tubes using Fresnel lenses.[73] That same year, Zhang's research team[74] employed orbital angular momentum beams to fabricate double-helical 3D microstructures, thereby demonstrating optical chirality.[74] In addition to the advancements mentioned above, the advancement of light field modulation techniques, including Bessel beams, Airy beams, Mathieu beams, and emerging

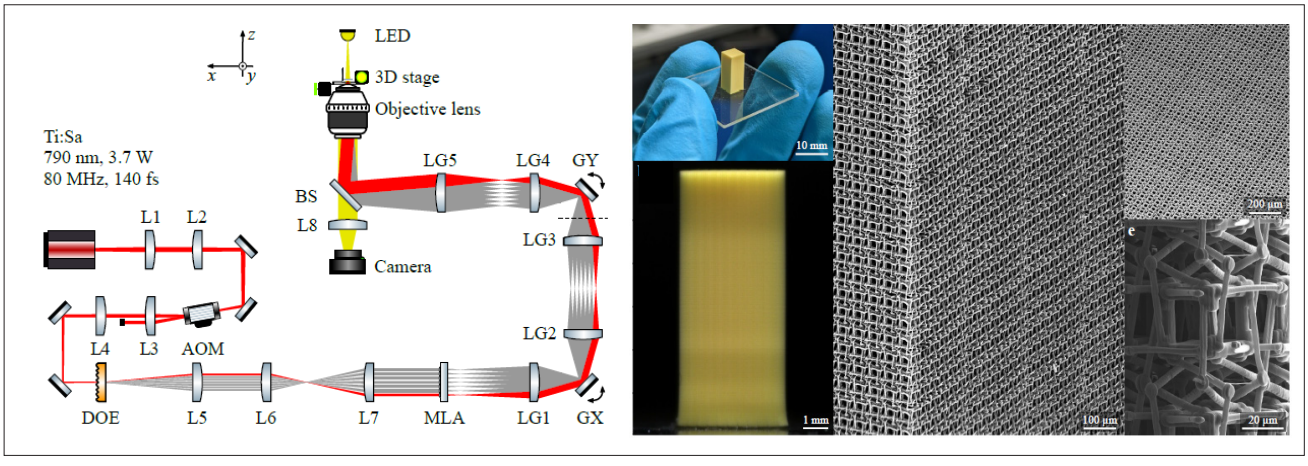

Figure 7. Multi-focal scanning based on a DOE and an MLA. Scale bars: 1 mm, 10 mm, 20 μm, and 200 μm. Reproduced with permission from Kiefer *et al.*[70] Abbreviations: 3D, three-dimensional; DOE, diffractive optical element; LED, light-emitting diode; MLA, micro lens array.

holographic technologies, has the potential to enable novel opportunities in micro-nano fabrication.[75–78]

4.2.2. Dynamic multi-foci or pattern exposure

In addition to static multi-focus, dynamic multi-focus or dynamic masking can be utilized to achieve more flexible fabrication, enabling greater versatility in structural manufacturing. The digital micromirror device (DMD) and liquid crystal spatial light modulator (LC-SLM) represent the two most widely utilized types of spatial light modulators, and Figure 8 illustrates their basic configurations within optical systems. Figure 8A illustrates the application of an LC-SLM for computational holography, Figure 8B demonstrates pattern projection through a 4-f system using a DMD, and Figure 8C illustrates binary holography with a DMD, utilizing a grating to compensate for the dispersion introduced by the DMD.

Parallel TPP based on beam-splitting devices has effectively enhanced efficiency, but still faces challenges in achieving precise control and remains confined to the production of periodic structures. SLM allows for greater flexibility in loading holograms and more precise manipulation of the light field. In 2007, Kelemen *et al.*[79] harnessed an LC-SLM to generate multiple foci, demonstrating the adaptability of programmable devices in creating multiple focal points.[79] Further optimization of the holograms improved the uniformity of the multi-foci, facilitating the fabrication of micro-nano optical devices and photonic crystal structures.[80] In 2024, Zhang's team[81] optimized focal point uniformity by suppressing zero-order spots and using a grayscale modulation strategy, reaching a peak printing rate of 1.49×10^8 voxels per second (Figure 9A).[81] Beyond generating multiple foci, different holograms loaded onto the SLM can enable scanning capabilities without requiring mechanical platform movement. In 2017, Yang *et al.*[82] introduced a fabrication strategy using non-diffractive superimposed Bessel beams. By adjusting the order of the superimposed Bessel light fields, they were able to control the number of foci generated. The complex 3D structures were fabricated by dynamically controlling the focal pattern.[82] In 2020, Manousidaki *et al.*[83] proposed a method for generating 3D holograms, which, by loading various holograms, enables the spatial movement of foci without mechanical platform motion, achieving efficiencies approximately 20 times greater than point-by-point scanning methods.[83] In 2022, Zhang *et al.*[84] successfully fabricated 3D structures through predesigned holograms integrated with lens phase modulation, eliminating the need for any movable components during the construction process (Figure 9B).[84]

DMDs function as innovative intensity control elements, offering a distinct advantage over LC-SLM. By rapidly flipping surface mirrors, they achieve binary modulation between "on" and "off" states, thus offering higher refresh rates.[85] The employment of grayscale holography has enabled efficient light field control, which is now successfully applied in areas such as beam shaping, pulse shaping, and two-photon microscopic imaging.[86–89]

In 2019, Geng *et al.*[90] developed a high-speed TPP system with multi-foci capabilities using Lee holography.

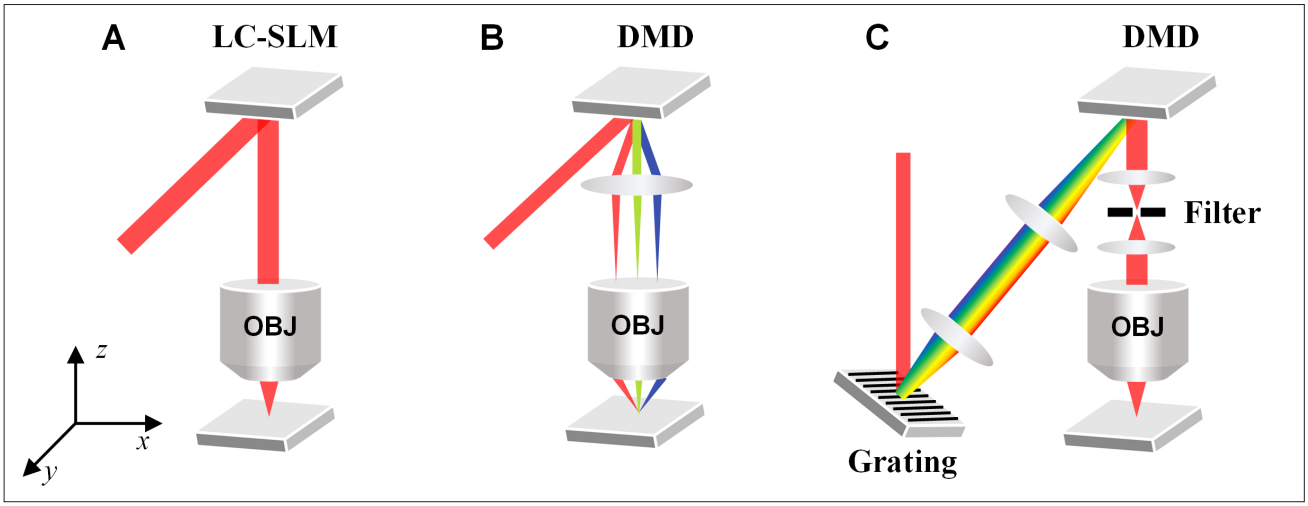

Figure 8. Dynamic modulation by spatial light modulators. (A) Computational holography utilizing LC-SLM. (B) Projection by DMD. (C) Binary holography implemented by DMD. Created by the authors with Microsoft PowerPoint. Abbreviations: DMD, digital micromirror device; LC-SLM, liquid crystal spatial light modulator; OBJ, objective.

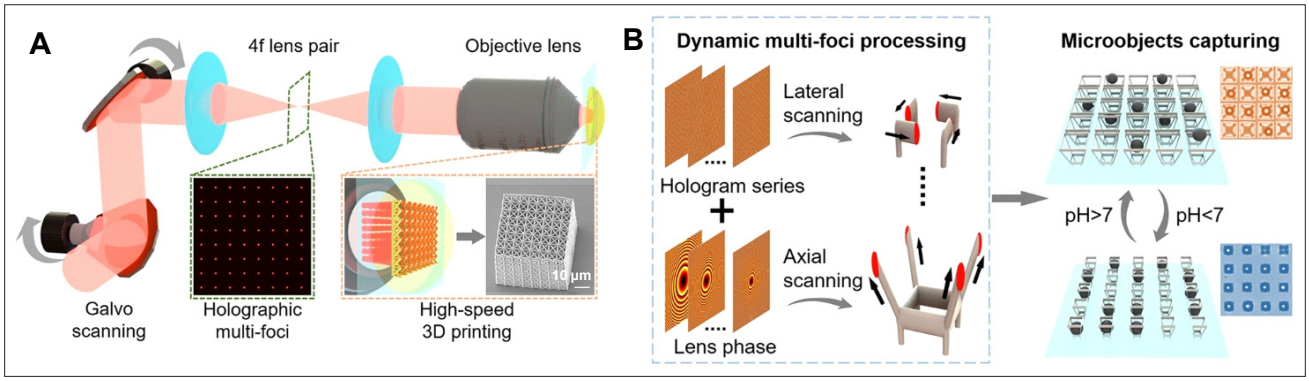

Figure 9. Multi-foci generated via spatial light modulators. (A) High-throughput two-photon polymerization enabled by holographic multi-foci high-speed scanning. Reproduced with permission from Zhang *et al.*[81] Copyright © 2024, American Chemical Society. (B) Microarchitectures fabricated by dynamic holographically shifted femtosecond multi-foci. Reproduced with permission from Zhang *et al.*[84] Copyright © 2022, American Chemical Society.

This system facilitated synchronous scanning that printed up to several foci, with a refresh rate of 22.7 kHz and a resolution of approximately 500 nm.[90] By 2023, this team had advanced to synchronously printing up to 2000 foci, achieving speeds of 2,000,000 voxels/s, and by analyzing polymerization dynamics, they reached a maximum resolution of 90 nm (Figure 10A).[91] In 2024, Jiao *et al.*[92] utilized a DMD as a digital mask, integrating an acousto-optic deflector with spatial light switching. The acousto-optic deflector driven by a non-linear swept signal significantly reduced the wavefront aberration. This approach not only achieved a printing rate of 7.6×10^7 voxels/s but also facilitated the fabrication of non-periodic structures (Figure 10B).[92]

The multi-foci parallel approach can significantly enhance throughput. The increase in laser power provides a basis for enabling patterned exposure through SLM. In 2014, Yang *et al.*[93] utilized an LC-SLM to generate large-format holographic patterns for the manufacture of specific patterns in a single exposure.[93] However, due to optical speckle noise, the printed surfaces lacked smoothness. That same year, the team introduced a multiple exposure technique that significantly improved the uniformity of the processed structures' surfaces, applying it to create high-quality DOE.[94] Although the multiple exposure method enhanced uniformity to some extent, it required the continuous loading of computed holograms to average out noise, thus reducing the throughput of the technique. In 2016, Zhang *et al.*[95] developed the mixed-region amplitude freedom holographic algorithm, which dramatically enhanced the quality of hologram generation, enabling high-quality single-exposure print formations. Fabricating masks with various patterns and projecting these designs through an optical system enables high-throughput manufacturing.[96–98] With the advancement of projection technology, DMD now enables the creation of adjustable 3D structures.[99,100] Beyond serving as a projection tool, DMD also functions as a dispersion element. By modulating the spatial chirp of a femtosecond laser pulse, the DMD confines a narrow pulse width exclusively to the sample locations, achieving synchronized spatio-temporal focusing. This method achieves an impressive lateral feature size of 140 nm and axial feature size of 170 nm, alongside high throughput in 3D micro-nano fabrication.[101,102] However, during the patterned exposure process, fluctuations in photochemical reaction intensities resulted in more proximity effects compared to point-by-point scanning methods, thus requiring an extended and meticulous process optimization.

5. High precision of two-photon polymerization

5.1. Processing parameters

The process parameters of TPP significantly influence fabrication precision. Figure 11 illustrates the typical workflow of TPP, encompassing direct writing, development, and drying. Adjusting these parameters can yield varying effects on the structures fabricated.

The feature size formed by TPP is influenced by both the optical diffraction limit and the threshold of polymer cross-linking. By regulating the light flux, the precision of the feature size can be improved, particularly when the scanning speed is high or the pulse energy is low. Moreover, when the spacing between two sets of cured structures is sufficiently small, re-polymerization occurs, resulting in finer lines. In 2007, Tan *et al.*[103] achieved line widths of less than 25 nm, merely 1/50 of the excitation wavelength, by modulating the light flux and increasing the scanning speed. By controlling the spacing between

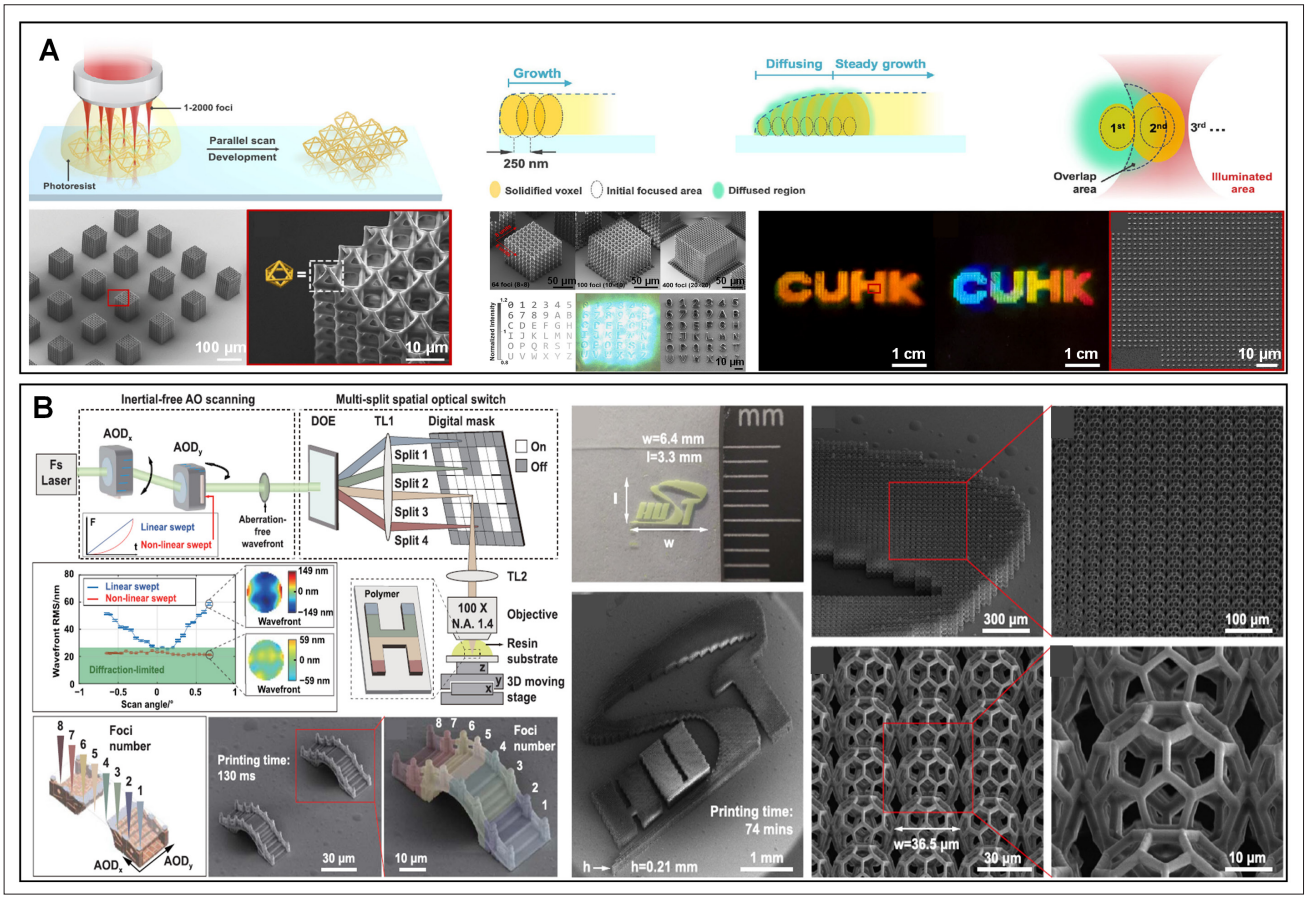

Figure 10. Employing a digital micromirror device for multi-foci parallel methods. (A) Efficient three-dimensional manufacturing facilitated by integrating polymerization dynamics. Scale bars: 1 cm, 10 μm, 50 μm, and 100 μm. Reproduced with permission from Ouyang *et al.*[91] (B) High-speed manufacturing through acousto-optic scanning integrated with spatial switching. Scale bars: 1 mm, 10 μm, 30 μm, and 300 μm. Reproduced with permission from Jiao *et al.*[92]

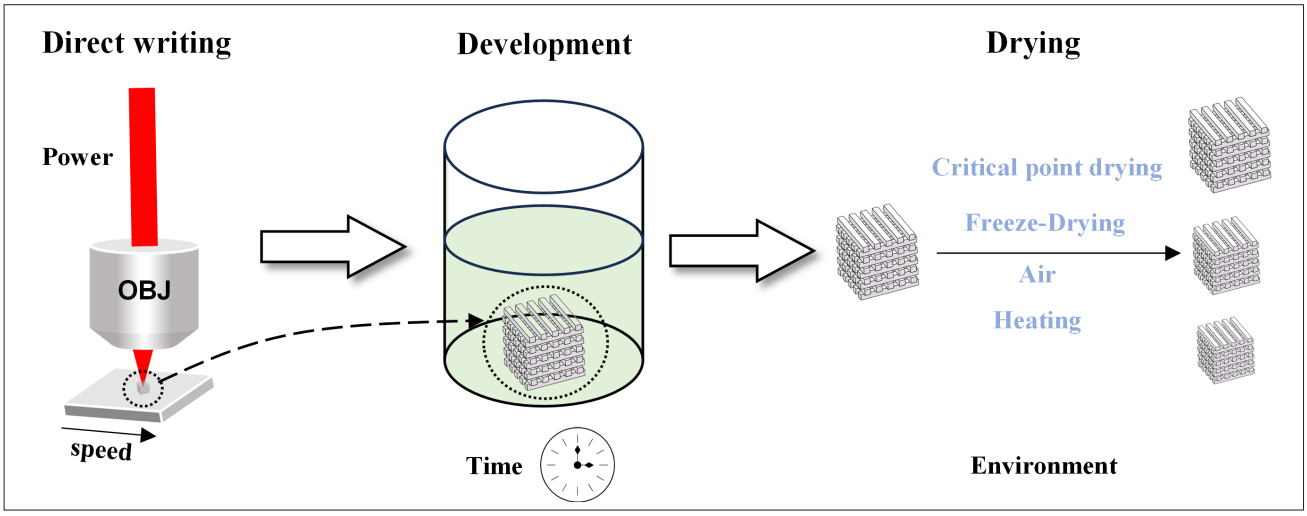

Figure 11. The workflow of two-point polymerization. Created by the authors with Microsoft PowerPoint. Abbreviation: OBJ, objective.

two sets of structures to induce re-polymerization, they achieved feature sizes of approximately 15 nm.[103]

However, solely controlling the laser dose also presents certain limitations. Firstly, the overall degree of cross-linking is low due to the reduced density of free radicals in the cross-linked regions, leading to weak structures that are prone to deformation during development and are insufficient to support 3D structures.[104] Secondly, this method does not reduce the spacing between lines. Although the feature size of a single line can be very small, free radicals persist around the lines. These free radicals are insufficient for monomer cross-linking, but when high-density patterns are inscribed, the residual free radicals accumulate, resulting in unintended structures.[105]

During the post-processing phase, the developer solution dissolves partially uncrosslinked structures, thereby reducing the feature size of the sample. The degree of cross-linking in TPP is typically below 75%, as demonstrated by Raman spectroscopy and Fourier transform infrared spectroscopy.[106–109] In this process, development time plays a crucial role. Insufficient time can result in residual ink remaining on the structure, while excessive time can compromise the structural integrity. Thus, the development duration must be carefully tailored to align with the properties of various ink types. In the drying process, capillary forces induce deformation in regions that lack sufficient strength to support the overall structure.[110] Additionally, certain materials, such as glass, necessitate the incorporation of nanoparticles into the photoresist for printing. The solid content of these nanoparticles in the photoresist is comparatively low. During the subsequent sintering process, the printed structures experience further shrinkage, resulting in an additional reduction in overall dimensions.[111]

In 2009, Maruo *et al.*[112] analyzed the overall structural shrinkage resulting from drying in air compared to that achieved with a critical point dryer.[112] Ovsianikov *et al.*[113] investigated the modifications in the photonic crystal bandgap under varying shrinkage ratios, indicating that shrinkage may be employed to enhance overall manufacturing precision.[113] In 2019, Liu *et al.*[114] introduced a heat-shrinking method to produce 3D-printed photonic crystals, achieving sub-100-nm features with a full range of colors (Figure 12).[114]

5.2. Optical systems

The optical system is crucial for the precision of the manufacturing systems. This section introduces several

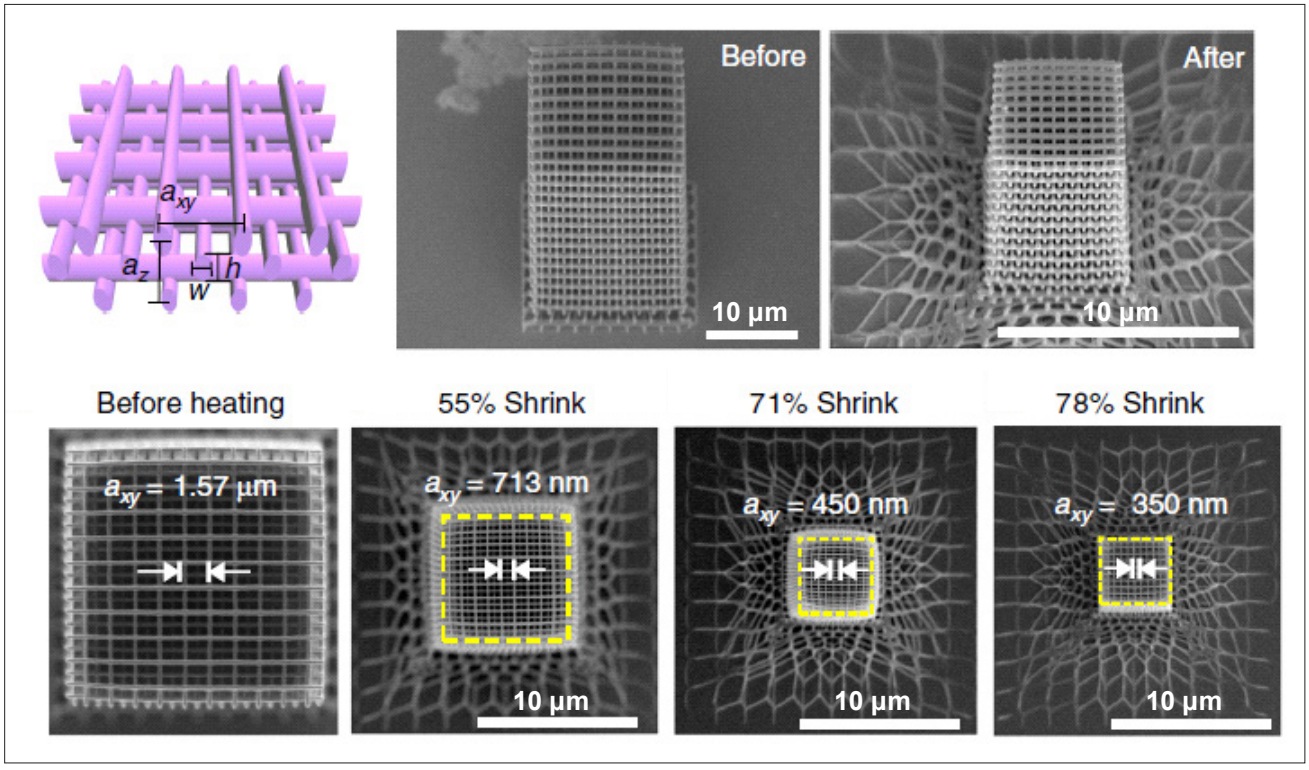

Figure 12. Variations in shrinkage after heating for different times. Scale bar: 10 μm. Reproduced with permission from Liu *et al.*[114]

methods to enhance precision based on optical imaging principles, as illustrated in Figure 13. These include reducing the wavelength, optimizing wavefront utilization (4Pi), and utilizing the properties of ultrafast lasers (spatiotemporal focusing).

According to the Rayleigh criterion, the diffraction limit of an optical system is defined by $\sigma = 0.61\lambda/\mathrm{NA}$, where λ represents the laser wavelength, and NA denotes the numerical aperture of the objective lens. Under fixed conditions for the objective lens, reducing the excitation light wavelength effectively diminishes the spot size, thereby enhancing resolution. Typically, the excitation wavelength of commonly used initiators in TPP is approximately 780 nm. Haske *et al.*[115] employed E,E-1,4-bis[4-(di-*n*-butylamino)styryl]-2,5-dimethoxybenzene as the initiator, exhibiting a two-photon absorption cross-section of 200 GM at 520 nm. By decreasing the wavelength, precision was significantly improved, ultimately achieving a linewidth of approximately 65 nm.[115] In 2022, Liu *et al.*[116] fabricated planar structures with a minimal feature size of 32 nm using DMD with an excitation wavelength of 400 nm.[116]

In super-resolution imaging, lateral resolution is typically enhanced, while axial resolution is approximately 2.5 times lower. Achieving isotropic resolution remains a significant scientific challenge. Generally, imaging with a single lens covers only half of the spherical wavefront; if the optical system could collect the other half behind the focal plane, the system's point spread function (PSF) would retain its spherical shape due to restored symmetry.[117] In 1992, Hell and colleagues[118] invented the 4Pi microscope using two opposing objective lenses, nearly capturing the entire 4Pi steradian angle.[118] The properties of micro/nanostructures fabricated using TPP are closely related to the smallest feature size of the voxel. Enhanced axial precision would improve the structural color exhibited by fabricated photonic crystals. In 2019, Tičkūnas *et al.*[119] proposed a TPP method based on 4Pi microscopy, significantly enhancing axial precision.[119] Using a 1030 nm laser, they achieved feature sizes of 200 nm laterally and 150 nm axially, resulting in nearly isotropic voxel features. Additionally, periodic layered structures can be directly fabricated using interference fringes formed in the axial direction.

In TPP fabrication, a voxel is the smallest unit. Its shape is directly related to the optical system's PSF. In single-photon absorption systems, the axial dimension of the PSF is typically about twice that of the lateral dimension. In contrast, femtosecond lasers offer richer temporal and frequency information than continuous lasers. This information can be utilized to effectively improve axial resolution. The product of the pulse width (τ_p) in the time domain and the spectral bandwidth ($\Delta\nu$) of a laser pulse, known as the time-bandwidth product, exceeds a specific constant κ, denoted by $\Delta\nu \cdot \tau_p \geq \kappa$. In 1985, Strickland and Mourou[120] proposed the chirped pulse amplification technique, which involves temporally stretching femtosecond pulses by separating the different

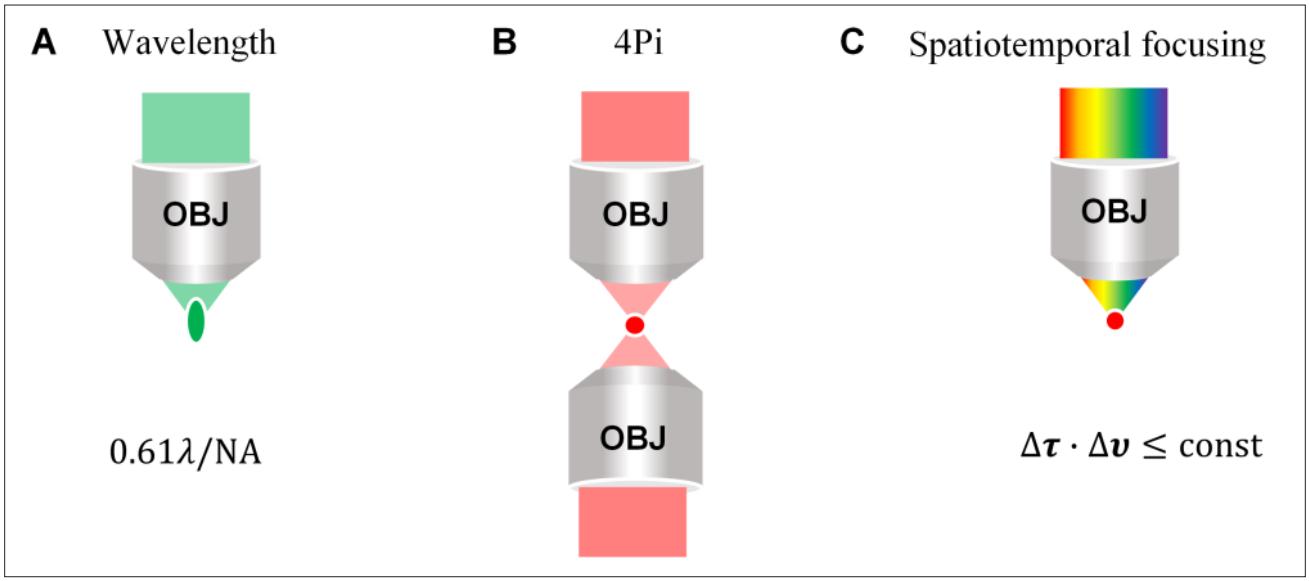

Figure 13. The enhancement of precision in two-photon polymerization through optical principles. (A) Reducing the wavelength of the laser. (B) Employing a 4Pi printing system. (C) Utilizing a spatiotemporal focusing system. Created by the authors with Microsoft PowerPoint. Abbreviation: OBJ, objective.

frequency components, thereby reducing peak power. After amplification, the pulses are then compressed. This technique was awarded the Nobel Prize in Physics in 2018. It fully exploits the temporal, spatial, and frequency characteristics of femtosecond pulses and has been widely applied in femtosecond laser-based technologies.

In two-photon imaging, the signal-to-noise ratio deteriorates with increased penetration depth. In 2005, Zhu's team[121] proposed a spatiotemporal focusing method. By broadening the femtosecond pulses with a grating to form spatial chirps and employing a 4f system during transmission, different frequency components converge at the focal point. Due to the time-bandwidth product, the peak power is insufficient to generate two-photon fluorescence signals after forming spatial chirps. However, at the focal point, the pulse width is minimized, achieving the focused pulse width necessary for effective two-photon fluorescence.[121] This method improves the PSF aspect ratio and enhances the axial precision of nonlinear optical systems. It has found broad applications in isotropic processing, two-photon imaging, and femtosecond laser filamentation.[122–125]

In 2010, an MIT research team utilized a mask and spatiotemporal focusing for high-throughput 3D printing. However, this method was confined to the fabrication of specific structures.[126] In 2012, Li *et al.*[127] used a DMD as a digital mask combined with spatiotemporal focusing for TPP (Figure 14A).[127] This approach entails a complex optical path due to the necessity of coupling the DMD with grating devices. In 2014, the team synchronized the DMD as a projection element and grating, achieving spatial light modulation and spatial chirp.[99] Despite this advancement, large-area manufacturing with DMD continued to encounter issues of inhomogeneous energy distribution and low structural precision. In 2017, Gu *et al.*[128] achieved uniform laser ablation using a beam homogenizer with spatiotemporal focusing, which resulted in a surface roughness not exceeding 96 nm.[128] By 2018, this system was applied to metal 3D printing.[129] In 2019, it enabled the rapid fabrication of nanoscale precision 3D structures, achieving up to 140 nm horizontal and 170 nm axial feature size, and improving manufacturing efficiency by more than three orders of magnitude compared to traditional point-by-point scanning methods.[101] In 2021, Somers' team[102] demonstrated the feasibility of this system for efficient large-scale micro- and nano-manufacturing (Figure 14B).[102] By 2022, Han's team[130] expanded this technology's precision using expansion microscopy, employing hydrogels as templates to assemble materials such as metals, two-dimensional materials, oxides, semiconductors, polymers, biological materials, and molecular crystals, achieving resolutions ranging from 20 to 200 nm in two-dimensional and 3D structures.[130]

This technology harnesses the temporal and spatial characteristics of femtosecond lasers, significantly enhancing precision and efficiency. It offers a novel technical direction for manufacturing cross-scale devices using TPP. However, due to the shift in processing paradigms, the fabrication of complex structures still necessitates substantial effort.[69,131–135]

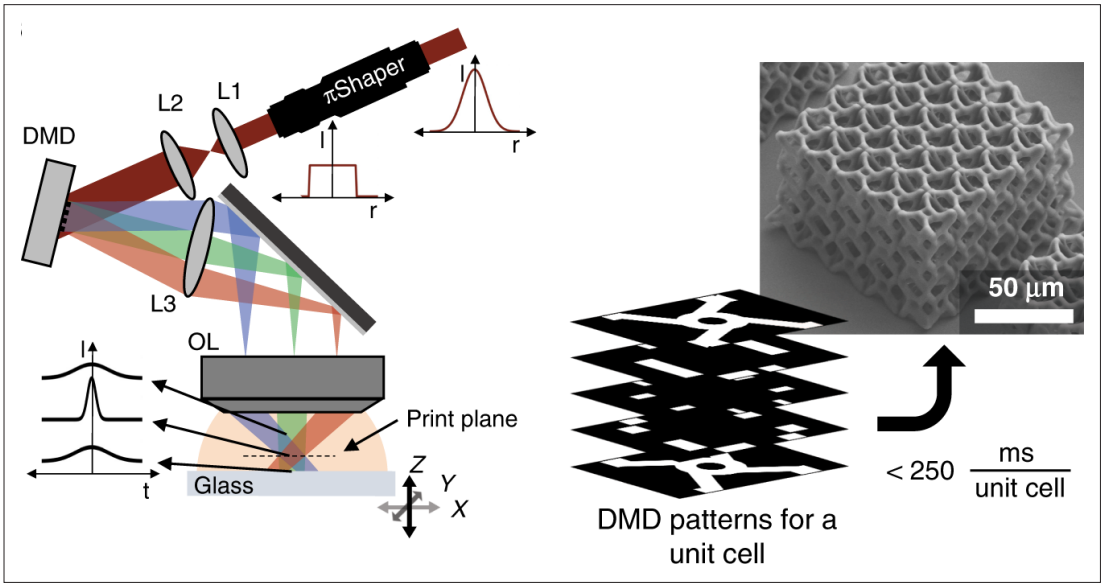

Figure 14. Spatiotemporal focusing in two-photon polymerization for the fabrication of metamaterials. Scale bar: 50 μm. Reproduced with permission from Somers *et al.*[102] Abbreviation: DMD, digital micromirror device.

5.3 Light–matter interactions

The TPP process involves both the optical system and the complex interactions between the laser and matter. By modulating the excited-state dynamics of the reaction system or modulating the interactions between ink components with light of varying wavelengths, it is possible to achieve higher precision in micro-nanostructure fabrication.

Hell[136] pioneered far-field super-resolution technology, specifically stimulated emission depletion (STED) microscopy. This technique utilizes the principle of reversible saturable optical linear fluorescence transition, which involves molecules that can reversibly switch between at least two states.[136] In 2014, this technique received the Nobel Prize in Chemistry, underscoring its significance. The process begins with exciting molecules to the excited state (λ_{exc}). If another beam (λ_{SE}) is applied before fluorescence emission, the excited molecules return to the ground state via stimulated emission, thereby reducing the rate of radiative transition. When both beams are coupled as Gaussian light, no signal is detected. However, when the excitation light is Gaussian and the depletion light is a vortex beam formed by a phase plate, their coupling effectively erases the PSF. This method has achieved a resolution of up to 2.4 nm, further highlighting its potential.[137] The mechanism and basic setup of STED are depicted in Figure 15.[138] Currently, methods that enhance precision through light–matter interactions are mainly inspired by STED technology. However, in their specific implementation, TPP and imaging techniques exhibit significant distinctions.

5.3.1. Kinetics

The kinetics, encompassing stimulated emission, electron transfer, triplet absorption, and photoisomerization, have been utilized in TPP. STED-assisted TPP was initially inspired by STED. By analyzing the excitation spectrum of the photoinitiator and selecting a wavelength close to its fluorescence spectrum for depletion, manufacturing precision is enhanced.[139] Unlike imaging techniques that prioritize the fluorescence quantum yield of fluorescent molecules—seeking the highest possible yield to minimize photobleaching and phototoxicity—TPP is inherently a photochemical reaction. It features a low fluorescence yield and a high ISC rate, allowing the photoinitiator molecules to participate more efficiently in chemical reactions. However, adapting STED from microscopy to lithography presents significant challenges to the material system.

The suppression of single-photon and TPP,[104,140] significantly promoted the application of STED in super-resolution lithography. However, the material systems still face limitations in fabricating complex 3D structures, including a slow response time and irreversible processes.[141] In 2010, Fischer *et al.*[139] introduced a photoresist based on the photoinitiator 2-isopropylthioxanthone (ITX), achieving results similar to stimulated emission depletion.[139] In 2011, using the same experimental setup, the group employed 7-diethylamino-3-thenoylcoumarin (DETC) as a photoinitiator to fabricate visible light photonic crystals, demonstrating the system's ultra-high resolution.[142] Compared to the reference, the region in the cloak exhibited invisibility under circular polarization illumination. In fact, beyond the expected stimulated emission pathway, when excited state molecules are exposed to depletion light, some excited state absorption or triplet state absorption may occur, which can increase polymerization probability, reduce depletion efficiency, and limit high-resolution performance.[143]

Photoresists for stimulated emission must possess a large oscillator strength for the S_0–S_1 transition, long excited state lifetimes, and high fluorescence quantum yields. A pump-probe experiment comparing ITX and DETC revealed that DETC exhibits a stronger

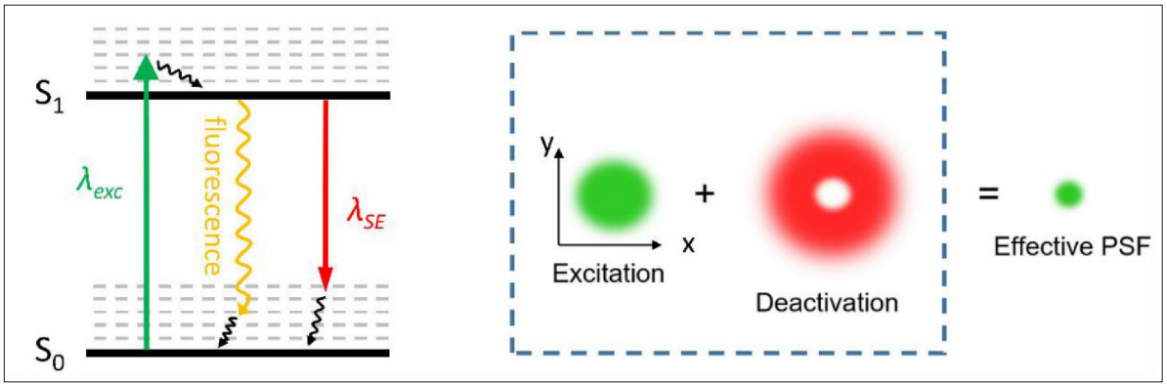

Figure 15. The Jablonski diagram and structural schematic of stimulated emission depletion microscopy. Reproduced with permission from Liaros and Fourkas.[138] Abbreviation: PSF, point spread function.

stimulated emission effect compared to its excited state absorption, making it more suitable as a photoinitiator for the stimulated emission mechanism.[144] Although ITX can achieve suppression in dual-color systems, it is not primarily driven by the stimulated emission process. DETC remains the leading photoinitiator supporting the stimulated emission suppression mechanism.[145] In 2013, Wollhofen *et al.* achieved a feature size of 55 nm and a resolution of 120 nm using DETC.[145] In 2015, Fischer *et al.* explored the mechanisms in STED-enhanced direct laser writing.[146]

With the advancement of this system, interest in enhancing the throughput of stimulated emission TPP has increased. In 2022, Zhu *et al.*[147] proposed a parallel peripheral-photoinhibition method by independently controlling the two polarization components of a light beam. They increased throughput while ensuring a minimum feature size of less than 40 nm (Figure 16).[147] To prevent the chromatic aberration of conventional multicolor inhibition lithography, they also developed single-color photoinhibition systems.[148,149]

The dual-color suppression method based on stimulated emission offers process reversibility. Additionally, the short fluorescence lifetime allows completion of this process within a nanosecond timescale, making it highly promising for high-throughput manufacturing.[150] However, given the short fluorescence lifetime, the stimulated emission rate must exceed the spontaneous emission rate, which demands high intensity for the depletion light, thereby increasing the method's cost and complexity.[151] The exploration of long-lived intermediate states to expand this approach warrants in-depth investigation.

The DETC inhibition mechanisms have been investigated in numerous studies. Fischer *et al.*[150] employed the pump-probe technique to analyze the efficacy of inhibition at various temporal delays. If the inhibition mechanism of DETC relies solely on stimulated emission, the inhibition timescale correlates with the molecule's inherent fluorescence lifetime, typically a few nanoseconds. Experimental findings revealed significant inhibition effects within nanoseconds post-pulse, which subsequently diminished. Furthermore, experiments indicated inhibition occurring before the excitation pulse, suggesting a residual impact from the previous pulse. This suggests that DETC's inhibition mechanism involves pathways additional to stimulated emission. In 2012, Harke *et al.*[152] explored the dynamics of super-resolution lithography polymerization, using a 642 nm laser that surpasses the fluorescence spectral range of ITX and DETC, discussing the possibility of ISC induced by triplet state absorption.[152] In these experiments, significant inhibition effects were observed even when the delay between the inhibition and excitation lights (800 ns for ITX and 5 μs for DETC) far exceeded the fluorescence lifetimes (0.1 ns–4 ns). To further analyze the triplet state processes, Harke *et al.*[153] conducted transient absorption studies on ITX and DETC, showing enhanced absorption rates over a prolonged duration at specific wavelengths. ITX absorbs at 630 nm, while DETC absorbs across a spectrum from visible to near-infrared.

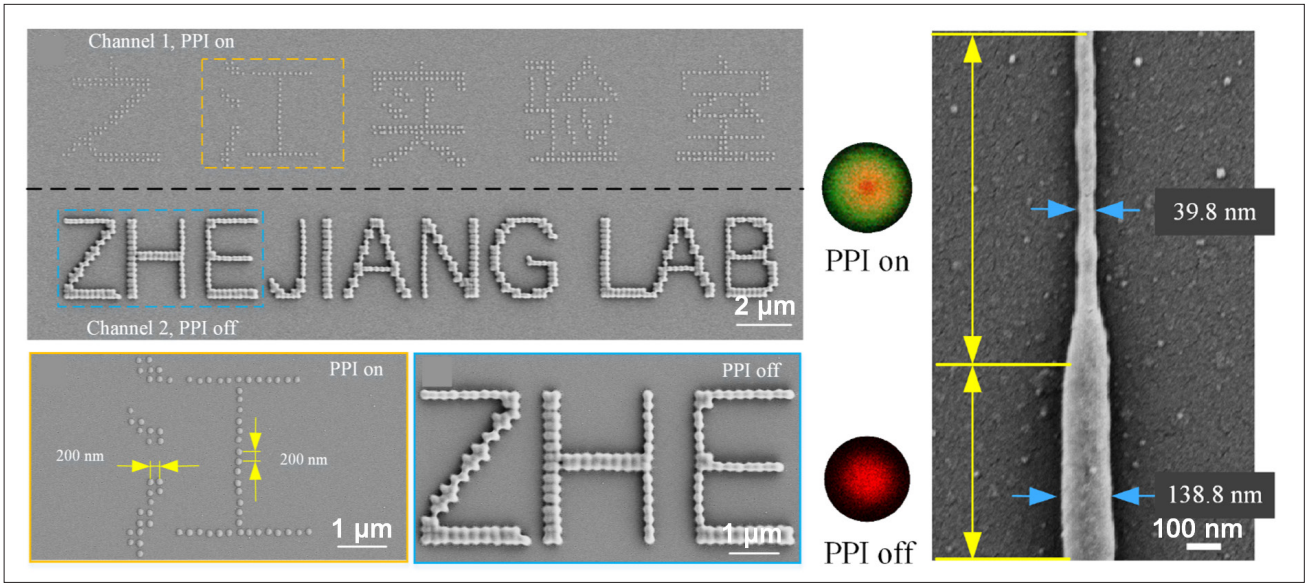

Figure 16. Enhancing two-photon polymerization precision through stimulated emission depletion microscopy. Scale bars: 1 μm, 2 μm, and 100 nm. Reproduced with permission from Zhu *et al.*[147]

Additionally, the discrete Fourier transform was utilized to calculate the triplet state absorption spectra of ITX and DETC, with the results aligning well with experimentally obtained photo-induced absorption spectra.[153] Thiel *et al.*[154] also successfully integrated the triplet state absorption in fabricating dual-band polarizers using a dip-in mode. Somers' team conducted a systematic study on DETC, examining the effects of co-initiators and various temporal delays, and confirming triplet state inhibition under an 808 nm laser (Figure 17).[155]

In 2009, Li *et al.*[140] first introduced the resolution augmentation through photoinduced deactivation (RAPID) technique for super-resolution lithography using a single-color light.[140] As dye molecules typically exhibit fluorescent lifetimes on the order of nanoseconds, subsequent studies have shown that the inhibitory time scale of this material system exceeds 13 ns, indicating that stimulated emission alone cannot account for this process. In 2011, Stocker and coworkers[156] proposed a self-inhibiting mechanism. In conventional photoresist systems, the degree of polymerization correlates directly with the laser dose; the slower the scanning speed, the greater the accumulation of light, and thus, the larger the polymer dimensions. However, an increased scanning speed paradoxically led to wider line widths, a phenomenon that classical excited-state dynamics models could not explain. To explain this process, they posited the solvent-stabilized electrons mechanism. After excitation to the excited state, the initiator undergoes ISC to the triplet state. Subsequently, molecules in the triplet state are converted into solvent-stabilized electrons and free radical cations, both of which can facilitate polymerization over extended periods. However, upon irradiation with an additional 800 nm light, the solvent-stabilized electrons and free radical cations recombine, resulting in the regeneration of the photoinitiator within photoresists based on the RAPID system. The method, owing to the extended lifetime of intermediate states, requires lower light power, thus enabling effective inhibition with relatively low-power continuous-wave lasers.

In two-color schemes, residual, partially cross-linked areas can persist if the suppression is not absolute, resulting in less than 100% effectiveness. These areas, though insufficient to reach the polymerization threshold, may overlap when constructing dense structures, leading to unwanted cross-linking. During the two-color suppression process, the excited state molecules influenced by the excitation light follow various pathways. The inhibition light suppresses some of these pathways, and when the inhibition light is strong, some non-suppressed pathways may be enhanced, ultimately compromising the suppression effect.[146] Decoupling the processes of polymerization and cross-linking can mitigate this issue and enhance resolution.[157] In 2018, Liaros *et al.*[157] proposed a three-color suppression scheme. Initially, using an 800 nm femtosecond laser, the material was pre-activated without directly inducing cross-linking. Similarly, illumination with a 445 nm continuous laser alone did

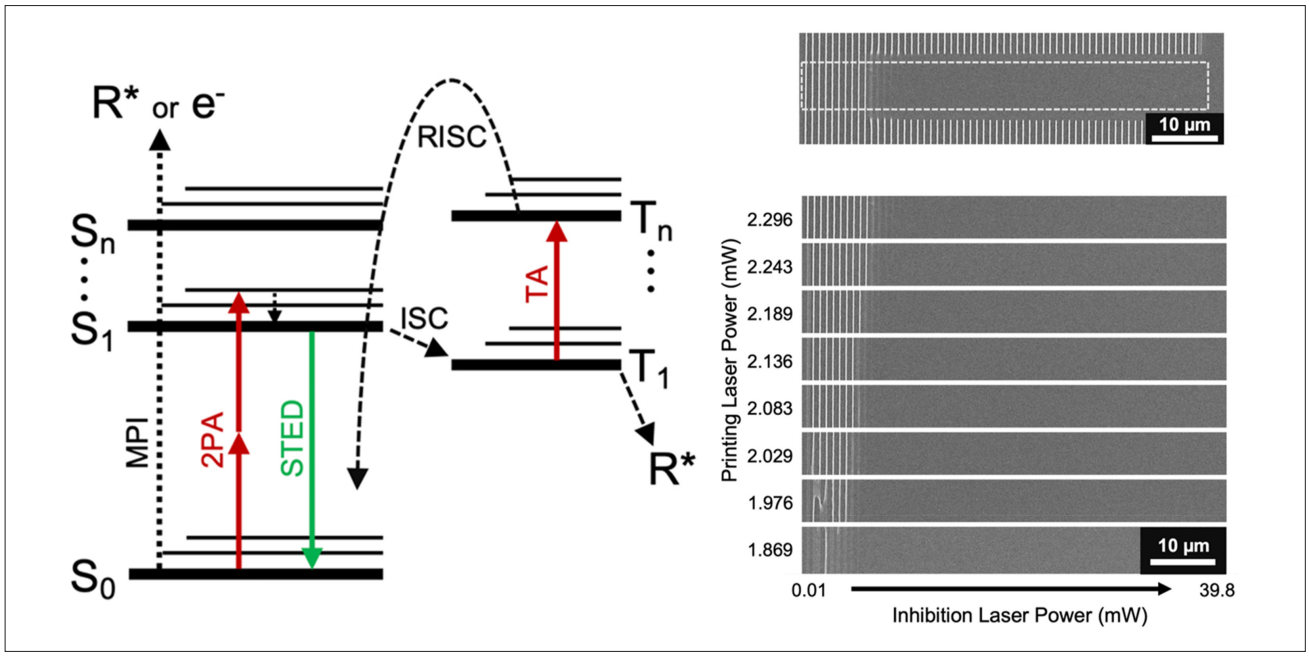

Figure 17. Experimental results of triplet state inhibition with DETC. Scale bar: 10 μm. Reproduced with permission from Somers *et al.*[155] Abbreviations: DETC, 7-diethylamino-3-thenoylcoumarin; ISC, intersystem crossing; RISC, reverse intersystem crossing; STED, stimulated emission depletion.

not lead to cross-linking. Cross-linking occurred only when both beams were applied simultaneously. A third beam was then introduced for inhibition. This process, by decoupling inhibition and cross-linking, significantly enhanced feature precision.

Photochromic materials provide a method to directly modulate either the transparency or the availability of monomers to light. Mueller *et al.*[158] proposed a super-resolution lithography technique using photoinduced isomerization. In 2017, they developed their method based on the cis-trans photoisomerization of intermediate photoenol species derived from α-methylbenzyl. In the presence of active enes, the E-enol undergoes a Diels–Alder reaction to form stable products. The short-lived Z-enol reverts to the original compound through a rapid reverse hydrogen transfer. By irradiating with 440 nm light, the E-enol is photoisomerized to Z-enol, inhibiting the formation of cyclic products and achieving a linewidth of 60 nm and resolution of 100 nm (Figure 18A).[158] In 2019, the team introduced a photoresist based on a methacrylic copolymer, with side chains composed of photochromic spirothiopyran moieties capable of forming crosslinks via supramolecular interactions between chromophores, achieving feature sizes as small as 31.2 nm (Figure 18B).[159] The variation in line thickness depicted in Figure 18 reflects the fabrication precision under two laser writing conditions: excitation light alone and the addition of quenching light.

5.3.2. Interactions among matter

In addition to regulating the behavior of individual components, light–matter interactions can also be employed to modulate the interaction between components. This approach can alter a material's light absorption properties and govern interactions between two kinds of molecules or between a molecule and the excited state of another type of molecule, ultimately achieving enhanced precision.

In 2009, Andrew and colleagues[160] utilized photochromic materials to achieve super-resolution lithography.[160] In their study, a layer of photochromic film, with two modes capable of absorbing either UV or visible light, was applied to the surface of a photoresist. Exposure to a specific light source toggled these molecules between an "OPEN" state, which absorbs ultraviolet light, and a "CLOSED" state, which absorbs visible light. This dynamic adjustment of the film's transparency to ultraviolet light narrowed the spatial distribution of ultraviolet exposure, enabling the etching of sub-wavelength-scale patterns. However, the method was limited by its relatively slow switching times and a finite number of adjustable cycles. The method of photoisomerization has broadened the dimensions of super-resolution lithography. However, challenges such as a slow photochromic response, low direct-write efficiency, and limited switching cycles persist. Enhancing the processing throughput of this system continues to be a significant area of research.

The mechanism of photoinhibition employs two distinct photonic pathways with different spatial distributions and wavelengths to initiate varied chemical reactions. One pathway promotes photopolymerization, while the other generates substances that lead to polymerization quenching. This photonic control of chemical reactions effectively suppresses the production of free radicals, thereby significantly enhancing the spatial resolution of printing. In 2009, Scott *et al.*[104] pioneered this technique, achieving processing precision beyond the diffraction limit. By shaping the inhibition light into a "doughnut" mode and overlaying it with the excitation light, they achieved lines as fine as 65 nm. However, the monomers used in the work polymerized slowly, and the

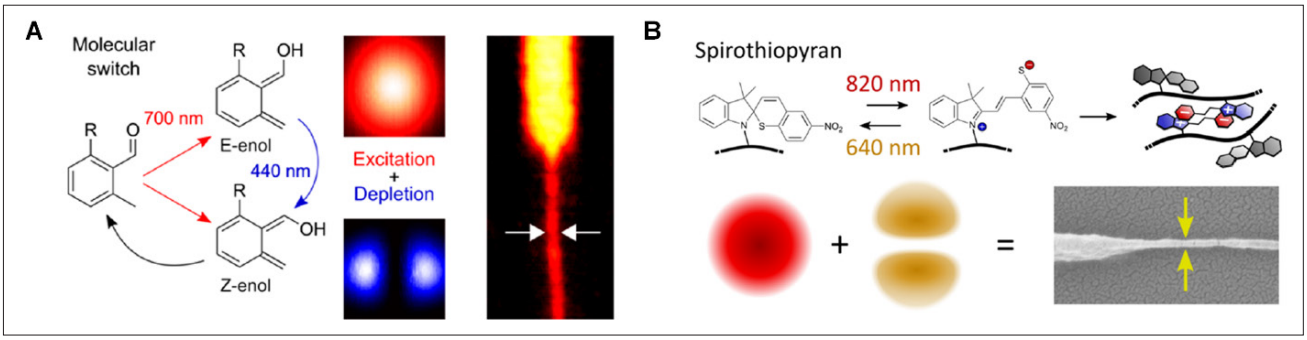

Figure 18. Enhancing two-photon polymerization precision through photoisomerization inhibition. (A) Achieving super-resolution through cis-trans isomerization of photoisomerization molecules. Reproduced with permission from Mueller *et al.*[158] Copyright © 2017, American Chemical Society. (B) Regulating crosslinking of photoisomerization molecules. Reproduced with permission from Müller *et al.*[159] Copyright © 2019, American Chemical Society.

cured modulus was relatively low, potentially leading to unforeseen precision loss. In 2011, Cao's team[161] employed BPE 100 photoresist, which boasts higher photosensitivity and modulus, to form voxels as small as 40 nm within an exposure time of 400 ms.[161] These studies were all based on single-photon absorption. In 2013, based on this system, Gan and coworkers[162] developed a method of TPP photoinduced dissipative inhibition. A lateral feature size of 9 nm is achieved by controlling the laser dose (Figure 19).[162] This technique requires relatively low power for the inhibition light, typically only at the milliwatt level, but its mechanism dictates an irreversibility that somewhat limits the development of this method.

A quencher, which is a traditional component in TPP inks, primarily inhibits radical diffusion and, as a result, improves precision. In 2024, Guan *et al.*[163] conducted an in-depth study on the relationship between initiators and quenchers, which revealed that 2,2,6,6-tetramethyl-4-piperidyl-1-oxyl efficiently quenches the excited state of DETC. They proposed a novel manufacturing approach based on the mutual suppression of light and matter, achieving an impressive precision of 30 nm, as illustrated in Figure 20.[163] The voxel sizes and throughputs have been extensively summarized in some articles.[70,81] Improved precision and higher throughput remain key trends in TPP. The performance and details of different TPP technologies are summarized in Figure 21 and Table 1.

Some techniques are very inspiring and show great feature sizes; however, they do not demonstrate the ability to fabricate 3D structures. Although these technologies are typically realized using polymer resins, they still face certain limitations before being fully applicable to biomedical fields. Biomedical materials such as gelatin methacryloyl and hyaluronic acid often require high biocompatibility or softness. Nevertheless, these technologies, as versatile platforms, offer promising new possibilities for biofabrication.

6. Conclusion

This paper provides a comprehensive overview of TPP in biomedical applications and explores advancements in TPP. Although TPP is a powerful micro-nanofabrication technique, its applications in biomedical engineering are still limited. In tissue engineering, constructing a 3D cell growth environment *in vitro* poses significant challenges in terms of manufacturing accuracy, material strength, and biocompatibility. Possible photodamage, along with the toxicity of substances in partially crosslinked materials, can significantly impact cell growth. Even if a micro-nano device exhibits good properties at the cellular level, for complex multi-level structures such as biological systems, cellular-level performance is difficult to directly guide macroscopic properties, thus necessitating higher manufacturing throughput. Taking human dental enamel as an example, this naturally occurring biomaterial, renowned for its exceptional hardness, stiffness, and toughness, provides valuable insights into the development of new medical materials and technologies. Dental enamel exemplifies a typical layered, multi-level structure; its primary components are hydroxyapatite nanowires (30–50 nm) tightly organized into enamel rods (4–6 μm), with the overall dimensions extending to the millimeter

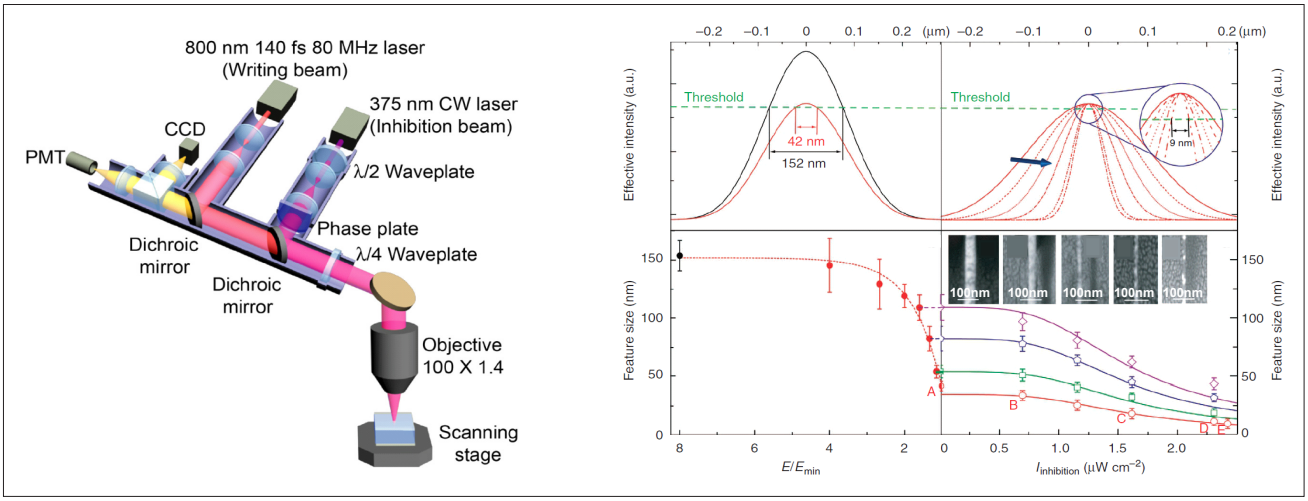

Figure 19. Enhancing the precision of two-photon polymerization through a photoinhibitor. Reproduced with permission from Gan *et al.*[162] Copyright © 2013, Springer Nature.

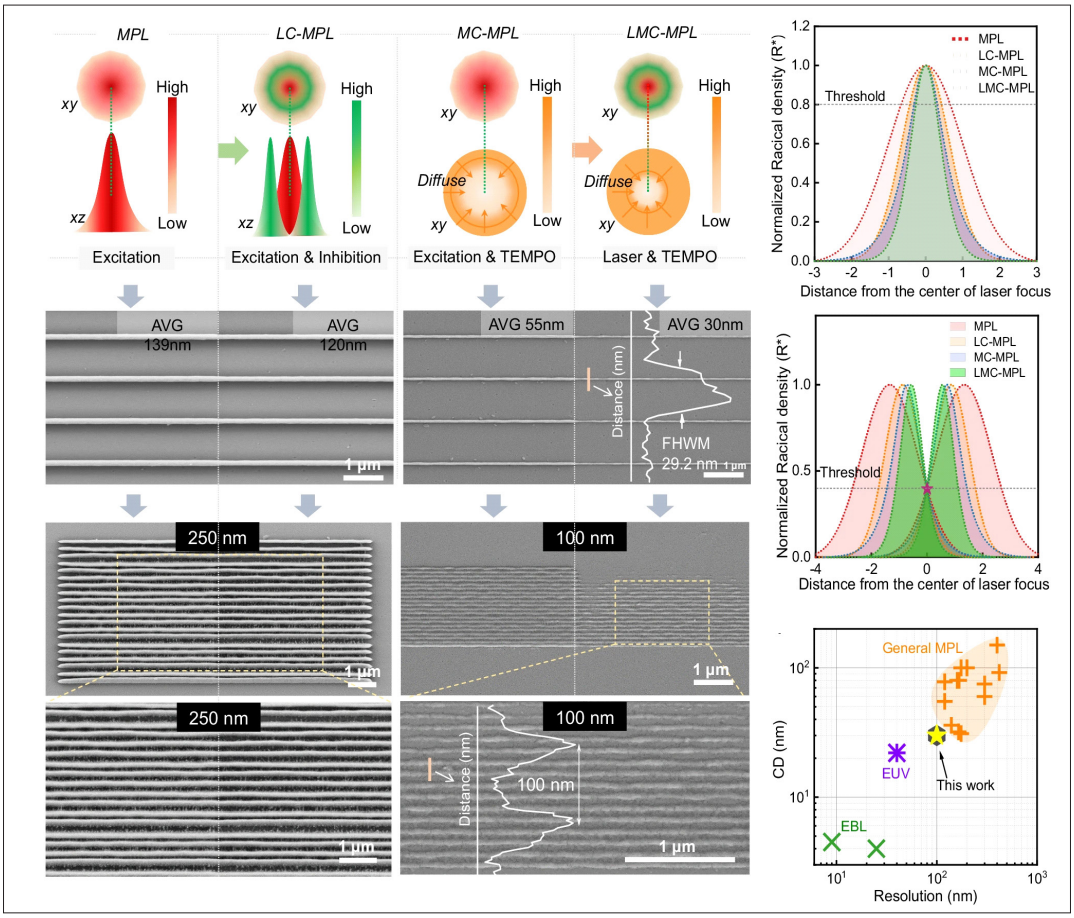

Figure 20. Light and matter co-confined multi-photon lithography. Scale bar: 1 μm. Reproduced with permission from Guan *et al.*[163] Abbreviations: EBL, E-beam lithography; EUV, extreme ultraviolet lithography; LC, light-confined; LMC, light and matter co-confined; MC, matter-confined; MPL, multi-photon lithography; TEMPO, 2,2,6,6-tetramethyl-4-piperidyl-1-oxyl

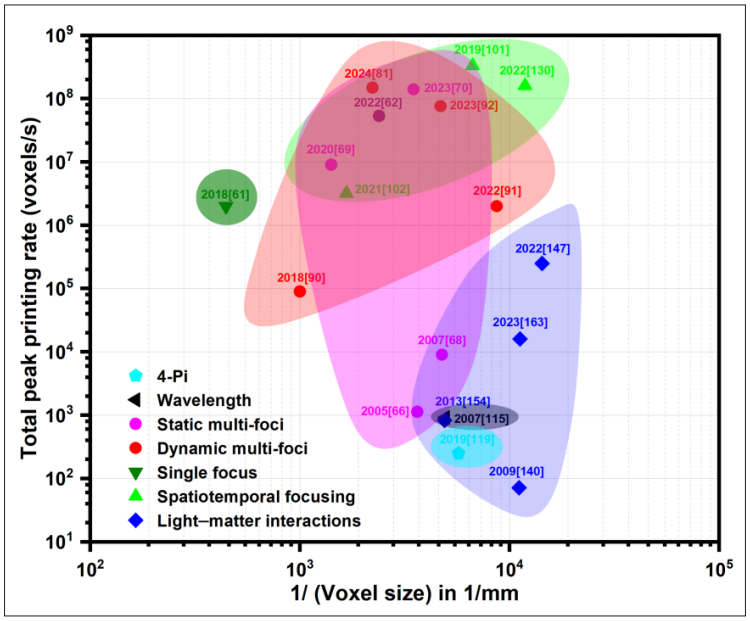

Figure 21. Comparison of various technologies based on their printing rate and voxel size. Created by the authors using Origin and Microsoft PowerPoint.

Table 1. Summary of two-photon polymerization efficiency and precision

Parameter		Approach	Feature size	Resolution	Speed	3D	Wavelength	Year	Ref
Efficiency	Serial scanning	Resonant-galvo mirror	1–4 μm (xy) 2 μm (z)	–	2×10^6 voxels/s	Yes	780 nm fs	2019	[61]
	Multi-foci	MLA	250 nm (xy)	–	1.13×10^3 voxels/s	Yes	799 nm fs	2005	[66]
		DOE + Galvo	120 nm (xy)	–	9×10^3 voxels/s	Yes	780 nm fs	2007	[68]
		DMD	500 nm (xy) 1500 nm (z)	–	9×10^4 voxels/s	Yes	800 nm fs	2019	[90]
		AOM + DOE + Galvo	406 nm (xy) 1010 nm (z)	–	9×10^6 voxels/s	Yes	790 nm fs	2020	[69]
		DMD	90 nm (xy) 141 nm (z)	–	2×10^6 voxels/s	Yes	800 nm fs	2023	[91]
		DMD	163 nm (xy) 263 nm (z)	220 nm (xy)	7.6×10^7 voxels/s	Yes	517 nm fs	2023	[92]
		DOE + MLA + Galvo	245 nm (xy) 328 nm (z)	–	1.4×10^8 voxels/s	Yes	790 nm fs	2024	[70]
		SLM + Galvo	215 nm (xy) 686 nm (z)	–	1.49×10^8 voxels/s	Yes	1,030 nm fs	2024	[81]
	Pattern	Projection	650 nm (xy) 10 μm (z)	–	1,000 patterns/s	No	800 nm fs	2013	[100]
		Computational holography	350 nm (xy)	–	200 patterns/s	No	800 nm fs	2016	[95]
	Light field	Bessel beam	Tube	–	2.5 structures/s	Yes	800 nm fs	2014	[73]
		OAM beam	Double-helix	–	10 sturctures/s	Yes	800 nm fs	2014	[74]
Precision	Processing Parameters	Laser dose	25 nm (xy)	–	700 μm/s	No	780 nm fs	2007	[103]
		Shrinkage	100 nm (xy)	–	200 μm/s	Yes	780 nm fs	2009	[113]
	Optical system	Wavelength	65 nm (xy) 340 nm (z)	500 nm (xy)	60 μm/s	Yes	520 nm fs	2007	[115]
			32 nm (xy)	165 nm (xy)	1 pattern/s	No	400 nm fs	2021	[116]
		4Pi	200 nm (xy) 150 nm (z)	–	50 μm/s	Yes	1030 nm fs	2020	[119]
		Spatiotemporal focusing	130–140 nm (xy) 170 nm (z)	–	3.33×10^8 voxels/s	Yes	800 nm fs	2019	[101]
			200 nm (xy) 1 um (z)	7 μm (z)	3.2×10^6 voxels/s	Yes	800 nm fs	2021	[102]
			20–200 nm (xy) 148.4 nm (z)	–	1.6×10^8 voxels/s	Yes	800 nm fs	2022	[130]

(Continue)

Table 1. Summary of two-photon polymerization efficiency and precision

Parameter		Approach	Feature size	Resolution	Speed	3D	Wavelength	Year	Ref
Precision	Laser-matter interaction	Photoinduced deactivation	40 nm (z)	–	10 μm/s	Yes	800 nm fs excitation 800 nm cw depletion	2009	[140]
		Stimulated emission depletion	–	175 nm (xy)	100 μm/s	No	810 nm fs excitation 532 nm cw depletion	2011	[143]
			40 nm (xy)	140 nm (xy)	1 mm/s	Yes	780 nm fs excitation 532 nm cw depletion	2022	[148]
			30 nm (xy) 148 nm (z)	100 nm (xy)	500 μm/s	Yes	525 nm fs excitation 532 nm ps depletion	2024	[163]
		Triplet state absorption	120 nm (xy) 288 nm (z)	525 nm (xy) 495 nm (z)	100 μm/s	Yes	780 nm fs excitation 639 nm cw depletion	2013	[154]
		Photoinhibitors	9 nm (xy)	52 nm (xy)	160 μm/s	No	800 nm fs excitation 375 nm cw depletion	2013	[162]
		Photoisomerization	60 nm (xy)	100 nm (xy)	10 μm/s	No	700 nm fs excitation 440 nm cw depletion	2017	[158]
			31.2 nm (xy)	175 nm (xy)	100 μm/s	Yes	820 nm fs excitation 640 nm cw depletion	2019	[159]
		Three-color strategy	101 nm (xy)	–	20–80 μm/s	No	800 nm fs preactivation 445 nm cw activation 800 nm cw deactivation	2018	[157]

Abbreviations: 3D, three-dimensional; AOM, acousto-optic modulator; DOE, diffractive optical element; DMD, digital micromirror device; MLA, micro lens array; OAM, orbital angular momentum of light; SLM, spatial light modulator.

doi: 10.36922/IJB025280281

scale.[3] Achieving a fully biomimetic, multi-level ordered structure requires exceedingly high precision, resolution, and throughput from manufacturing technologies. Current methods, while achieving high precision, often struggle to maintain adequate physical, mechanical, and optical properties. Furthermore, limited by proximity effects, replicating the naturally densely packed structure is challenging. To overcome these obstacles, efforts can include, but should not be restricted to, the following strategies.

Optically, advanced optical measurement technology can be integrated with TPP to enable high-precision manufacturing and facilitate real-time feedback. Some technologies, such as two-photon fluorescence imaging, optical coherence tomography, optical diffraction tomography, STED, 4Pi, and expansion microscopy, have been incorporated into the process.[119,127,130,140,164,165] Moreover, certain approaches involving polar coordinates and volumetric additive manufacturing also hold promising potential in TPP.[166,167] TPP devices share structural similarities with many imaging systems. Imaging technology primarily focuses on information extraction. Optical signals contain multidimensional information, including time, space, frequency, and polarization. It enables the observation of the dynamic processes of the micro-robots and facilitates an understanding of the principles governing their motion.[168] Furthermore, new light–material interaction mechanisms are also necessary to broaden the range of material applications.

Chemically, a more comprehensive analysis of the properties of photoresists is required, encompassing both their steady-state and transient behaviors. Besides the nonlinearity induced by the femtosecond laser, higher-order nonlinear effects during the chemical reactions initiated by different photoinitiators necessitate diverse analytical techniques. Steady-state methods like Fourier transform infrared spectroscopy, Raman, and coherent anti-Stokes Raman scattering spectroscopy analyze polymerization process and kinetics, while time-resolved scattering and transient absorption spectroscopy examine transient phenomena.[10,153] Additionally, kinetic models of different photoresist systems enable precise manufacturing predictions through multi-physical field coupling models using new computational methods.[163] For instance, COMSOL models reaction kinetics, MATLAB assesses the impact of various kinetic processes, and molecular dynamics analyzes experimentally challenging scenarios.[109,169,170]

From a materials perspective, broadening the range of functional materials and designing high-performance photoinitiators remain critical objectives. To address diverse applications, researchers have proposed various strategies. For instance, coating polymer surfaces with nickel and titanium enhances magnetic control and biocompatibility of these devices, depositing metals on polymer surfaces enhances the electric field for biosensing, and integrating silica nanospheres within polymers creates highly transparent glass structures. Moreover, exploring visible-light photoinitiators offers potential to further reduce phototoxicity and enable the application of TPP in bioprinting.

In summary, TPP technology holds significant research and practical value across multiple domains. By exploring its primary development directions and technical features, this paper underscores its indispensable role in biomedicine. As throughput and efficiency improve, TPP will increasingly impact the fabrication of advanced interventional medical devices, single-cell interaction studies, organ-on-chip research, and the development of hierarchical materials.

Acknowledgments

We acknowledge support by Beijing Advanced Innovation Center for Biomedical Engineering.

Funding

This study was funded National Natural Science Foundation of China (92477111, 22073003), Beijing Natural Science Foundation (L232109), Fundamental Research Funds for the Central Universities (YWF-22-K101).

Conflict of interest

Jiebo Li is a Guest Editor of this special issue, but was not in any way involved in the editorial and peer-review process conducted for this paper, directly or indirectly. Separately, other authors declared that they have no known competing financial interests or personal relationships that could have influenced the work reported in this paper.

Author contributions

Conceptualization: Yanzhe Fu, Bosong Yu
Visualization: Yanzhe Fu, Mingming Huang, Jiayong Wei
Writing-original draft: Yanzhe Fu, Mingming Huang, Jiebo Li
Writing–review & editing: Xiang Ding, Jiebo Li, Jianmin Han, Lizhen Wang, Yubo Fan

Ethics approval and consent to participate

Not applicable.

Consent for publication

Not applicable.

Availability of data

Not applicable.

References

1. Khademhosseini A, Langer R. Microengineered hydrogels for tissue engineering. *Biomaterials*. 2007;28(34):5087-5092. doi: 10.1016/j.biomaterials.2007.07.021.
2. Asadollahbaik A, Thiele S, Weber K, *et al*. Highly efficient dual-fiber optical trapping with 3D printed diffractive fresnel lenses. *ACS Photonics*. 2020;7(1):88-97. doi: 10.1021/acsphotonics.9b01024.
3. Zhao H, Liu S. Liu S, Wei Y, *et al*. Multiscale engineered artificial tooth enamel. *Science*. 2022;375 (6580):551-556. doi: 10.1126/science.abj3343
4. Kawata S, Sun H-B, Tanaka T, *et al*. Finer features for functional microdevices. *Nature*. 2001;412(6848):697-698. doi: 10.1038/35089130.
5. Greant C, Van Durme B, Van Hoorick J, *et al*. Multiphoton lithography as a promising tool for biomedical applications. *Adv Funct Mater*. 2023;33(39):202212641. doi: 10.1002/adfm.202212641.
6. Arslan A, Steiger W, Roose P, *et al*. Polymer architecture as key to unprecedented high-resolution 3D-printing performance: the case of biodegradable hexa-functional telechelic urethane-based poly-ε-caprolactone. *Mater Today*. 2021;44:25-39. doi: 10.1016/j.mattod.2020.10.005.
7. Song J, Michas C, Chen CS, *et al*. From simple to architecturally complex hydrogel scaffolds for cell and tissue engineering applications: opportunities presented by two-photon polymerization. *Adv Healthc Mater*. 2020;9(1):e1901217. doi: 10.1002/adhm.201901217.
8. Zipfel WR, Williams RM, Webb WW. Nonlinear magic: multiphoton microscopy in the biosciences. *Nat Biotechnol*. 2003;21(11):1369-1377. doi: 10.1038/nbt899.
9. Somers P, Münchinger A, Maruo S, *et al*. The physics of 3D printing with light. *Nat Rev Phys*. 2023;6:99-113. doi: 10.1038/s42254-023-00671-3.
10. Mueller JB, Fischer J, Mayer F, *et al*. Polymerization kinetics in three-dimensional direct laser writing. *Adv Mater*. 2014;26(38):6566-6571. doi: 10.1002/adma.201402366.
11. Fischer J, Mueller JB, Kaschke J, *et al*. Three-dimensional multi-photon direct laser writing with variable repetition rate. *Opt Express*. 2013;21(22):26244-26260. doi: 10.1364/OE.21.026244.
12. Balena A, Bianco M, Pisanello F, *et al*. Recent advances on high-speed and holographic two-photon direct laser writing. *Adv Funct Mater*. 2023;33(39). doi: 10.1002/adfm.202211773.
13. Maruo S, Nakamura O, Kawata S. Three-dimensional microfabrication with two-photon-absorbed photopolymerization. *Opt Lett*. 1997;22(2):132-134. doi: 10.1364/OL.22.000132.
14. Langer R, Vacanti JP. Tissue engineering. *Science*. 1993;260(5110):920-926. doi: 10.1126/science.8493529.
15. Chan BP, Leong KW. Scaffolding in tissue engineering: general approaches and tissue-specific considerations. *Eur Spine J*. 2008;17(4):467-479. doi: 10.1007/s00586-008-0745-3.
16. Chung S, Ingle NP, Montero GA, *et al*. Bioresorbable elastomeric vascular tissue engineering scaffolds via melt spinning and electrospinning. *Acta Biomater*. 2010;6(6):1958-1967. doi: 10.1016/j.actbio.2009.12.007.
17. Liu X, Ma PX. Phase separation, pore structure, and properties of nanofibrous gelatin scaffolds. *Biomaterials*. 2009;30(25):4094-4103. doi: 10.1016/j.biomaterials.2009.04.024.
18. Sin D, Miao X, Liu G, *et al*. Polyurethane (PU) scaffolds prepared by solvent casting/particulate leaching (SCPL) combined with centrifugation. *Mater Sci Eng C*. 2010;30(1):78-85. doi: 10.1016/j.msec.2009.09.002.
19. Amensag S, McFetridge PS. Tuning scaffold mechanics by laminating native extracellular matrix membranes and effects on early cellular remodeling. *J Biomed Mater Res A*. 2014;102(5):1325-1333. doi: 10.1002/jbm.a.34791.
20. Li X, Lu W, Xu X, *et al*. Advanced optical methods and materials for fabricating 3D tissue scaffolds. *Light Adv Manuf*. 2022;3(3):1. doi: 10.37188/lam.2022.026.
21. Lee J-Y, An J, Chua CK. Fundamentals and applications of 3D printing for novel materials. *Appl Mater Today*. 2017;7:120-133. doi: 10.1016/j.apmt.2017.02.004.
22. Chia HN, Wu BM. Recent advances in 3D printing of biomaterials. *J Biol Eng*. 2015;9(1):4. doi: 10.1186/s13036-015-0001-4.
23. Zandrini T, Shan O, Parodi V, *et al*. Multi-foci laser microfabrication of 3D polymeric scaffolds for stem cell expansion in regenerative medicine. *Sci Rep*. 2019;9(1):11761. doi: 10.1038/s41598-019-48080-w.
24. Torgersen J, Qin X-H, Li Z, *et al*. Hydrogels for two-photon polymerization: a toolbox for mimicking the extracellular matrix. *Adv Funct Mater*. 2013;23(36):4542-4554. doi: 10.1002/adfm.201203880.

25. Ovsianikov A, Schlie S, Ngezahayo A, *et al*. Two-photon polymerization technique for microfabrication of CAD-designed 3D scaffolds from commercially available photosensitive materials. *J Tissue Eng Regen Med*. 2007;1(6):443-449.
doi: 10.1002/term.57.

26. Klein F, Striebel T, Fischer J, *et al*. Elastic fully three-dimensional microstructure scaffolds for cell force measurements. *Adv Mater*. 2010;22(8):868-871.
doi: 10.1002/adma.200902515.

27. Klein F, Richter B, Striebel T, *et al*. Two-component polymer scaffolds for controlled three-dimensional cell culture. *Adv Mater*. 2011;23(11):1341-1345.
doi: 10.1002/adma.201004060.

28. Ricci D, Nava MM, Zandrini T, *et al*. Scaling-up techniques for the nanofabrication of cell culture substrates via two-photon polymerization for industrial-scale expansion of stem cells. *Materials*. 2017;10(1):66.
doi: 10.3390/ma10010066.

29. Turunen S, Joki T, Hiltunen ML, *et al*. Direct laser writing of tubular microtowers for 3D culture of human pluripotent stem cell-derived neuronal cells. *ACS Appl Mater Interfaces*. 2017;9(31):25717-25730.
doi: 10.1021/acsami.7b05536.

30. Lemma ED, Spagnolo B, Rizzi F, *et al*. Microenvironmental stiffness of 3D polymeric structures to study invasive rates of cancer cells. *Adv Healthc Mater*. 2017;6(22):1700888.
doi: 10.1002/adhm.201700888.

31. Tudor A, Delaney C, Zhang H, *et al*. Fabrication of soft, stimulus-responsive structures with sub-micron resolution via two-photon polymerization of poly(ionic liquid)s. *Mater Today*. 2018;21(8):807-816.
doi: 10.1016/j.mattod.2018.07.017.

32. Marino A, Tricinci O, Battaglini M, *et al*. A 3D real-scale, biomimetic, and biohybrid model of the blood-brain barrier fabricated through two-photon lithography. *Small*. 2018;14(6).
doi: 10.1002/smll.201702959.

33. Fendler C, Denker C, Harberts J, *et al*. Microscaffolds by direct laser writing for neurite guidance leading to tailor-made neuronal networks. *Adv Biosyst*. 2019;3(5):1800329.
doi: 10.1002/adbi.201800329.

34. Akolawala Q, Rovituso M, Versteeg HH, *et al*. Evaluation of proton-induced DNA damage in 3D-engineered glioblastoma microenvironments. *ACS Appl Mater Interfaces*. 2022;14(18):20778-20789.
doi: 10.1021/acsami.2c03706.

35. Rengaraj A, Bosc L, Machillot P, *et al*. Engineering of a microscale niche for pancreatic tumor cells using bioactive film coatings combined with 3D-architectured scaffolds. *ACS Appl Mater Interfaces*. 2022;14(11):13107-13121.
doi: 10.1021/acsami.2c01747.

36. Costa BNL, Adao RMR, Maibohm C, *et al*. Cellular interaction of bone marrow mesenchymal stem cells with polymer and hydrogel 3D microscaffold templates. *ACS Appl Mater Interfaces*. 2022;14(11):13013-13024.
doi: 10.1021/acsami.1c23442.

37. Kaushik S, Hord AH, Denson DD, *et al*. Lack of pain associated with microfabricated microneedles. *Anesth. Analg*. 2001;92(2):502-504.
doi: 10.1213/00000539-200102000-00041.

38. Ovsianikov A, Chichkov B, Mente P, *et al*. Two photon polymerization of polymer–ceramic hybrid materials for transdermal drug delivery. *Int J Appl Ceram Technol*. 2007;4(1):22-29.
doi: 10.1111/j.1744-7402.2007.02115.x.

39. Prausnitz MR, Langer R, Transdermal drug delivery. *Nat Biotechnol*. 2008;26(11):1261-1268.
doi: 10.1038/nbt.1504.

40. Faraji Rad Z, Nordon RE, Anthony CJ, *et al*. High-fidelity replication of thermoplastic microneedles with open microfluidic channels. *Microsyst Nanoeng*. 2017;3(1):17034.
doi: 10.1038/micronano.2017.34.

41. Balmert SC, Carey CD, Falo GD, *et al*. Dissolving undercut microneedle arrays for multicomponent cutaneous vaccination. *J Controlled Release*. 2020;317:336-346.
doi: 10.1016/j.jconrel.2019.11.023.

42. Li J, Thiele S, Quirk BC, *et al*. Ultrathin monolithic 3D printed optical coherence tomography endoscopy for preclinical and clinical use. *Light Sci Appl*. 2020;9(1):124.
doi: 10.1038/s41377-020-00365-w.

43. Lee S, Kim JY, Kim J, *et al*. A needle-type microrobot for targeted drug delivery by affixing to a microtissue. *Adv Healthc Mater*. 2020;9(7):e1901697.
doi: 10.1002/adhm.201901697.

44. Yang T, Si T, Wu Y, *et al*. Breaking the limitation of laminar flow in thrombolytic therapy with reconfigurable vortex-like nanobot swarms. *Angew Chem Int Ed*. 2025;64(17):e202425189.
doi: 10.1002/anie.202425189.

45. Wrede P, Remlova E, Chen Y, *et al*. Synergistic integration of materials in medical microrobots for advanced imaging and actuation. *Nat Rev Mater*. 2025.
doi: 10.1038/s41578-025-00811-4.

46. Ren L, Nama N, McNeill JM, *et al*. 3D steerable, acoustically powered microswimmers for single-particle manipulation. *Sci Adv*. 2019;5(10):eaax3084.
doi: 10.1126/sciadv.aax3084.

47. Li D, Liu Y, Yang Y, *et al*. A fast and powerful swimming microrobot with a serrated tail enhanced propulsion interface. *Nanoscale*. 2018;10(42):19673-19677.
doi: 10.1039/c8nr04907f.

48. Huang T-Y, Huang H-W, Jin DD, *et al*. Four-dimensional micro-building blocks. *Sci Adv*. 2020;6(3):eaav8219.

doi: 10.1126/sciadv.aav8219.

49. Han H, Ma X, Deng W, *et al*. Imaging-guided bioresorbable acoustic hydrogel microrobots. *Sci Robot*. 2024;9(97):eadp3593. doi: 10.1126/scirobotics.adp3593.

50. Papanikolaou EG, D'Haeseleer E, Verheyen G, *et al*. Live birth rate is significantly higher after blastocyst transfer than after cleavage-stage embryo transfer when at least four embryos are available on day 3 of embryo culture. A randomized prospective study. *Hum. Reprod*. 2005;20(11):3198-203. doi: 10.1093/humrep/dei217.

51. Medina-Sanchez M, Schwarz L, Meyer AK, *et al*. Cellular cargo delivery: toward assisted fertilization by sperm-carrying micromotors. *Nano Lett*. 2016;16(1):555-561. doi: 10.1021/acs.nanolett.5b04221.

52. Fan J, Ren S, Han B, *et al*. Magnetic fiber robots with multiscale functional structures at the distal end. *Adv Funct Mater*. 2023;34(12). doi: 10.1002/adfm.202309424.

53. Wang X, Qin XH, Hu C, *et al*. 3D printed enzymatically biodegradable soft helical microswimmers. *Adv Funct Mater*. 2018;28(45):1804107. doi: 10.1002/adfm.201804107.

54. Ceylan H, Yasa IC, Yasa O, *et al*. 3D-printed biodegradable microswimmer for theranostic cargo delivery and release. *ACS Nano*. 2019;13(3):3353-3362. doi: 10.1021/acsnano.8b09233.

55. Oellers M, Lucklum F, Vellekoop MJ. On-chip mixing of liquids with swap structures written by two-photon polymerization. *Microfluid Nanofluidics*. 2019;24(1):4. doi: 10.1007/s10404-019-2309-8.

56. Lölsberg J, Linkhorst J, Cinar A, *et al*. 3D nanofabrication inside rapid prototyped microfluidic channels showcased by wet-spinning of single micrometre fibres. *Lab Chip*. 2018;18(9):1341-1348. doi: 10.1039/C7LC01366C.

57. Jiménez-Zenteno AK, Estève A, Cayron H, *et al*. A novel 3D microdevice for the in vivo capture of cancer-associated cells. *Med Devices Sens*. 2019;2(5–6):e10056. doi: 10.1002/mds3.10056.

58. Lao Z, Zheng Y, Dai Y, *et al*. Nanogap plasmonic structures fabricated by switchable capillary-force driven self-assembly for localized sensing of anticancer medicines with microfluidic SERS. *Adv Funct Mater*. 2020;30(15): 1909467. doi: 10.1002/adfm.201909467.

59. Erfle P, Riewe J, Bunjes H, *et al*. Goodbye fouling: a unique coaxial lamination mixer (CLM) enabled by two-photon polymerization for the stable production of monodisperse drug carrier nanoparticles. *Lab Chip*. 2021;21(11): 2178-2193. doi: 10.1039/D1LC00047K.

60. Michas C, Karakan MÇ, Nautiyal P, *et al*. Engineering a living cardiac pump on a chip using high-precision fabrication. *Sci Adv*. 2022;8(16):eabm3791. doi: 10.1126/sciadv.abm3791.

61. Pearre BW, Michas C, Tsang JM, *et al*. Fast micron-scale 3D printing with a resonant-scanning two-photon microscope. *Addit Manuf*. 2019;30:100887. doi: 10.1016/j.addma.2019.100887.

62. Kuroiwa Y, Takeshima N, Narita Y, *et al*. Arbitrary micropatterning method in femtosecond laser microprocessing using diffractive optical elements. *Opt Express*. 2004;12(9):1908-1915. doi: 10.1364/OPEX.12.001908.

63. Hasegawa S, Hayasaki Y, Nishida N. Holographic femtosecond laser processing with multiplexed phase Fresnel lenses. *Opt Lett*. 2006;31(11):1705-1707. doi: 10.1364/OL.31.001705.

64. Yamaji M, Kawashima H, Suzuki Ji, *et al*. Three dimensional micromachining inside a transparent material by single pulse femtosecond laser through a hologram. *Appl Phys Lett*. 2008;93(4):041116. doi: 10.1063/1.2965451.

65. Wang X, Fan X, Liu Y, *et al*. 3D nanolithography via holographic multi-focus metalens. *Laser Photonics Rev*. 2024;18(11). doi: 10.1002/lpor.202400181.

66. Kato J-i, Takeyasu N, Adachi Y, *et al*. Multiple-spot parallel processing for laser micronanofabrication. *Appl Phys Lett*. 2005;86(4):044102. doi: 10.1063/1.1855404.

67. Jesacher A, Booth MJ. Parallel direct laser writing in three dimensions with spatially dependent aberration correction. *Opt Express*. 2010;18(20):21090-21099. doi: 10.1364/OE.18.021090.

68. Dong X-Z, Zhao Z-S, Duan X-M. Micronanofabrication of assembled three-dimensional microstructures by designable multiple beams multiphoton processing. *Appl Phys Lett*. 2007;91(12):124103. doi: 10.1063/1.2789661.

69. Hahn V, Kiefer P, Frenzel T, *et al*. Rapid assembly of small materials building blocks (voxels) into large functional 3D metamaterials. *Adv Funct Mater*. 2020;30(26):1907795. doi: 10.1002/adfm.201907795.

70. Kiefer P, Hahn V, Kalt S, *et al*. A multi-photon (7 × 7)-focus 3D laser printer based on a 3D-printed diffractive optical element and a 3D-printed multi-lens array. *Light Adv Manuf*. 2024;4(1):28-41. doi: 10.37188/lam.2024.003.

71. Ježek J, Čižmár T, Neděla V, *et al*. Formation of long and thin polymer fiber using nondiffracting beam. *Opt Express*. 2006;14(19):8506-8515. doi: 10.1364/OE.14.008506.

72. Stankevicius E, Gertus T, Rutkauskas M, *et al*. Fabrication of micro-tube arrays in photopolymer SZ2080 by using three different methods of a direct laser polymerization technique. *J Micromech Microeng*. 2012;22(6):065022. doi: 10.1088/0960-1317/22/6/065022.

73. Zhang C, Hu Y, Li J, *et al*. A rapid two-photon fabrication of tube array using an annular Fresnel lens. *Opt Express*. 2014;22(4):3983-3990. doi: 10.1364/OE.22.003983.

74. Zhang S-J, Li Y, Liu Z-P, *et al*. Two-photon polymerization of a three dimensional structure using beams with orbital angular momentum. *Appl Phys Lett*. 2014;105(6):061101. doi: 10.1063/1.4893007.

75. Pan D, Liu S, Ji S, *et al*. Efficient fabrication of a high-aspect-ratio AFM tip by one-step exposure of a long focal depth holographic femtosecond axilens beam. *Opt Lett*. 2020;45(4):897-900. doi: 10.1364/OL.384249.

76. Wang C, Rao R, Cai Z, *et al*. Microclaw array fabricated by single exposure of femtosecond airy beam and self-assembly for regulating cell migratory plasticity. *ACS Nano*. 2023;17(10):9025-9038. doi: 10.1021/acsnano.2c11577.

77. Wang C, Yang L, Hu Y, *et al*. Femtosecond Mathieu beams for rapid controllable fabrication of complex microcages and application in trapping microobjects. *ACS Nano*. 2019;13(4):4667-4676. doi: 10.1021/acsnano.9b00893.

78. Dorrah AH, Bordoloi P, de Angelis VS, *et al*. Light sheets for continuous-depth holography and three-dimensional volumetric displays. *Nat Photonics*. 2023;17(5):427-434. doi: 10.1038/s41566-023-01188-y.

79. Kelemen L, Valkai S, Ormos P. Parallel photopolymerisation with complex light patterns generated by diffractive optical elements. *Opt Express*. 2007;15(22):14488-14497. doi: 10.1364/OE.15.014488.

80. Yang L, El-Tamer A, Hinze U, *et al*. Parallel direct laser writing of micro-optical and photonic structures using spatial light modulator. *Opt Lasers Eng*. 2015;70:26-32. doi: 10.1016/j.optlaseng.2015.02.006.

81. Zhang L, Wang C, Zhang C, *et al*. High-throughput two-photon 3D printing enabled by holographic multi-foci high-speed scanning. *Nano Lett*. 2024;24(8):2671-2679. doi: 10.1021/acs.nanolett.4c00505.

82. Yang L, Qian D, Xin C, *et al*. Two-photon polymerization of microstructures by a non-diffraction multifoci pattern generated from a superposed Bessel beam. *Opt Lett*. 2017;42(4):743-746. doi: 10.1364/OL.42.000743.

83. Manousidaki M, Papazoglou DG, Farsari M, *et al*. 3D holographic light shaping for advanced multiphoton polymerization. *Opt Lett*. 2020;45(1):85-88. doi: 10.1364/OL.45.000085.

84. Zhang L, Liu B, Wang C, *et al*. Functional shape-morphing microarchitectures fabricated by dynamic holographically shifted femtosecond multifoci. *Nano Lett*. 2022;22(13):5277-5286. doi: 10.1021/acs.nanolett.2c01178.

85. Dudley D, Duncan W, Slaughter J. Emerging digital micromirror device (DMD) applications. Proceedings of SPIE; 2003:4985. doi: 10.1117/12.480761.

86. Cheng J, Gu C, Zhang D, *et al*. High-speed femtosecond laser beam shaping based on binary holography using a digital micromirror device. *Opt Lett*. 2015;40(21):4875-4878. doi: 10.1364/OL.40.004875.

87. Cheng J, Gu C, Zhang D, *et al*. Ultrafast axial scanning for two-photon microscopy via a digital micromirror device and binary holography. *Opt Lett*. 2016;41(7):1451-1454. doi: 10.1364/OL.41.001451.

88. Gu C, Zhang D, Chang Y, *et al*. Digital micromirror device-based ultrafast pulse shaping for femtosecond laser. *Opt Lett*. 2015;40(12):2870-2873. doi: 10.1364/OL.40.002870.

89. Geng Q, Gu C, Cheng J, *et al*. Digital micromirror device-based two-photon microscopy for three-dimensional and random-access imaging. *Optica*. 2017;4(6):674-677. doi: 10.1364/OPTICA.4.000674.

90. Geng Q, Wang D, Chen P, *et al*. Ultrafast multi-focus 3-D nano-fabrication based on two-photon polymerization. *Nat Commun*. 2019;10(1):2179. doi: 10.1038/s41467-019-10249-2.

91. Ouyang W, Xu X, Lu W, *et al*. Ultrafast 3D nanofabrication via digital holography. *Nat Commun*. 2023;14(1):1716. doi: 10.1038/s41467-023-37163-y.

92. Jiao BJ, Chen F, Liu Y, *et al*. Acousto-optic scanning spatial-switching multiphoton lithography. *Int J Extreme Manuf*. 2023;5(3):035008. doi: 10.1088/2631-7990/ace0a7.

93. Yang L, Li J, Hu Y, *et al*. Projection two-photon polymerization using a spatial light modulator. *Opt Commun*. 2014;331:82-86. doi: 10.1016/j.optcom.2014.05.051.

94. Zhang C, Hu Y, Li J, *et al*. An improved multi-exposure approach for high quality holographic femtosecond laser patterning. *Appl Phys Lett*. 2014;105(22):221104. doi: 10.1063/1.4902925.

95. Zhang C, Hu Y, Du W, *et al*. Optimized holographic femtosecond laser patterning method towards rapid integration of high-quality functional devices in microchannels. *Sci Rep*. 2016;6(1):33281. doi: 10.1038/srep33281.

96. Kaehr B, Shear JB. Multiphoton fabrication of chemically responsive protein hydrogels for microactuation. *Proc Natl Acad Sci*. 2008;105(26):8850-8854. doi: 10.1073/pnas.0709571105.

97. Kaehr B, Shear JB. Mask-directed multiphoton lithography. *J Am Chem Soc*. 2007;129(7):1904-1905. doi: 10.1021/ja068390y.

98. Kaehr B, Shear JB. High-throughput design of microfluidics based on directed bacterial motility. *Lab Chip*. 2009;9(18):2632-2637. doi: 10.1039/B908119D.

99. Yih J-N, Hu YY, Sie YD, *et al*. Temporal focusing-based multiphoton excitation microscopy via digital micromirror device. *Opt Lett*. 2014;39(11):3134-3137. doi: 10.1364/OL.39.003134.

100. Mills B, Grant-Jacob JA, Feinaeugle M, *et al*. Single-pulse multiphoton polymerization of complex structures using a digital multimirror device. *Opt Express*. 2013;21(12):14853-14858. doi: 10.1364/OE.21.014853.

101. Saha SK, Wang D, Nguyen VH, *et al*. Scalable submicrometer additive manufacturing. *Science*. 2019;366(6461): 105-109. doi: 10.1126/science.aax8760.

102. Somers P, Liang Z, Johnson JE, *et al*. Rapid, continuous projection multi-photon 3D printing enabled by spatiotemporal focusing of femtosecond pulses. *Light Sci Appl*. 2021;10(1):199. doi: 10.1038/s41377-021-00645-z.

103. Tan D, Li Y, Qi F, *et al*. Reduction in feature size of two-photon polymerization using SCR500. *Appl Phys Lett*. 2007;90(7):071106. doi: 10.1063/1.2535504.

104. Scott TF, Kowalski BA, Sullivan AC, *et al*. Two-color single-photon photoinitiation and photoinhibition for subdiffraction photolithography. *Science*. 2009;324(5929):913-917. doi: 10.1126/science.1167610.

105. Fischer J, Wegener M. Three-dimensional optical laser lithography beyond the diffraction limit. *Laser Photonics Rev*. 2013;7(1):22-44. doi: 10.1002/lpor.201100046.

106. Baldacchini T, Zimmerley M, Kuo CH, *et al*. Characterization of microstructures fabricated by two-photon polymerization using coherent anti-stokes Raman scattering microscopy. *J Phys Chem B*. 2009;113(38):12663-12668. doi: 10.1021/jp9058998.

107. Cicha K, Li Z, Stadlmann K, *et al*. Evaluation of 3D structures fabricated with two-photon-photopolymerization by using FTIR spectroscopy. *J Appl Phys*. 2011;110(6):064911. doi: 10.1063/1.3639304.

108. Jiang LJ, Zhou YS, Xiong W, *et al*. Two-photon polymerization: investigation of chemical and mechanical properties of resins using Raman microspectroscopy. *Opt Lett*. 2014;39(10):3034-3037. doi: 10.1364/OL.39.003034.

109. Sedghamiz E, Liu M, Wenzel W. Challenges and limits of mechanical stability in 3D direct laser writing. *Nat Commun*. 2022;13(1):2115. doi: 10.1038/s41467-022-29749-9.

110. Li Y, Qi FJ, Yang HH, *et al*. Nonuniform shrinkage and stretching of polymerized nanostructures fabricated by two-photon photopolymerization. *Nanotechnology*. 2008;19(5):055303. doi: 10.1088/0957-4484/19/05/055303.

111. Wen X, Zhang B, Wang W, *et al*. 3D-printed silica with nanoscale resolution. *Nat Mater*. 2021;20(11): 1506-1511. doi: 10.1038/s41563-021-01111-2.

112. Maruo S, Hasegawa T, Yoshimura N. Single-anchor support and supercritical CO2 drying enable high-precision microfabrication of three-dimensional structures. *Opt Express*. 2009;17(23):20945-20951. doi: 10.1364/OE.17.020945.

113. Ovsianikov A, Shizhou X, Farsari M, *et al*. Shrinkage of microstructures produced by two-photon polymerization of Zr-based hybrid photosensitive materials. *Opt Express*. 2009;17(4):2143-2148. doi: 10.1364/OE.17.002143.

114. Liu Y, Wang H, Ho J, *et al*. Structural color three-dimensional printing by shrinking photonic crystals. *Nat Commun*. 2019;10(1):4340. doi: 10.1038/s41467-019-12360-w.

115. Haske W, Chen VW, Hales JM, *et al*. 65 nm feature sizes using visible wavelength 3-D multiphoton lithography. *Opt Express*. 2007;15(6):3426-3436. doi: 10.1364/OE.15.003426.

116. Liu YH, Zhao YY, Jin F, *et al*. Lambda/12 super resolution achieved in maskless optical projection nanolithography for efficient cross-scale patterning. *Nano Lett*. 2021;21(9):3915-3921. doi: 10.1021/acs.nanolett.1c00559.

117. Hao X, Li Y, Fu S, *et al*. Review of 4Pi fluorescence nanoscopy. *Engineering*. 2022;11:146-153. doi: 10.1016/j.eng.2020.07.028.

118. Hell S, Stelzer EHK. Properties of a 4Pi confocal fluorescence microscope. *J Opt Soc Am A*. 1992;9(12):2159-2166. doi: 10.1364/JOSAA.9.002159.

119. Tičkūnas T, Paipulas D, Purlys V. 4Pi multiphoton polymerization. *Appl Phys Lett*. 2020;116(3):031101. doi: 10.1063/1.5128786.

120. Strickland D, Mourou G. Compression of amplified chirped optical pulses. *Opt Commun*. 1985;55(6):447-449. doi: 10.1016/0030-4018(85)90151-8.

121. Zhu G, Howe Jv, Durst M, *et al*. Simultaneous spatial and temporal focusing of femtosecond pulses. *Opt Express*. 2005;13(6):2153-2159. doi: 10.1364/OPEX.13.002153.

122. Papagiakoumou E, de Sars V, Oron D, *et al*. Patterned two-photon illumination by spatiotemporal shaping of ultrashort pulses. *Opt Express*. 2008;16(26):22039-22047. doi: 10.1364/OE.16.022039.

123. He F, Xu H, Cheng Y, *et al*. Fabrication of microfluidic channels with a circular cross section using spatiotemporally focused femtosecond laser pulses. *Opt Lett*. 2010;35(7):1106-1108. doi: 10.1364/OL.35.001106.

124. Vitek DN, Adams DE, Johnson A, *et al*. Temporally focused femtosecond laser pulses for low numerical aperture micromachining through optically transparent materials. *Opt Express*. 2010;18(17):18086-18094. doi: 10.1364/OE.18.018086.

125. Chu W, Tan Y, Wang P, *et al*. Centimeter-height 3D printing with femtosecond laser two-photon polymerization. *Adv Mater Technol*. 2018;3(5):1700396. doi: 10.1002/admt.201700396.

126. Kim D, So PTC. High-throughput three-dimensional lithographic microfabrication. *Opt Lett*. 2010;35(10):1602-1604. doi: 10.1364/ol.35.001602.

127. Li YC, Cheng LC, Chang CY, *et al*. Fast multiphoton microfabrication of freeform polymer microstructures by spatiotemporal focusing and patterned excitation. *Opt Express*. 2012;20(17):19030-19038. doi: 10.1364/oe.20.019030.

128. Gu C, Zhang D, Wang D, *et al*. Parallel femtosecond laser light sheet micro-manufacturing based on temporal focusing. *Precis Eng*. 2017;50:198-203. doi: 10.1016/j.precisioneng.2017.05.006.

129. Wang D, Wen C, Chang Y, *et al*. Ultrafast laser-enabled 3D metal printing: a solution to fabricate arbitrary submicron metal structures. *Precis. Eng*. 2018;52:106-111. doi: 10.1016/j.precisioneng.2017.11.015.

130. Han F, Gu S, Klimas A, *et al*. Three-dimensional nanofabrication via ultrafast laser patterning and kinetically regulated material assembly. *Science*. 2022;378(6626):1325-1331. doi: 10.1126/science.abm8420.

131. Saha SK, Chen S-C. Comment on "Rapid Assembly of Small Materials Building Blocks (Voxels) into Large Functional 3D Metamaterials". *Adv Funct Mater*. 2020;30(30):2001060. doi: 10.1002/adfm.202001060.

132. Kim H, Pingali R, Saha SK. Rapid printing of nanoporous 3D structures by overcoming the proximity effects in projection two-photon lithography. *Virtual Phys Prototyp*. 2023;18(1):e2230979. doi: 10.1080/17452759.2023.2230979.

133. Johnson JE, Jamil IR, Pan L, *et al*. Bayesian optimization with Gaussian-process-based active machine learning for improvement of geometric accuracy in projection multi-photon 3D printing. *Light Sci Appl*. 2025;14(1):56. doi: 10.1038/s41377-024-01707-8.

134. Fu Y, Wang B, Wei J, *et al*. Single-step and parallel high-speed fabrication for Au micro-/nanostructures. *Opt Lett*. 2024;49(21):6001-6004. doi: 10.1364/ol.539524.

135. Fu Y, Li N, Ding X, *et al*. Medium-assisted scalable printing of LIPSS via femtosecond laser projection manufacturing. *Opt Lett*. 2025;50(3):844-847. doi.: 10.1364/OL.549389.

136. Hell SW. Far-field optical nanoscopy. *Science*. 2007;316(5828):1153-1158. doi: 10.1126/science.1137395.

137. Wildanger D, Patton BR, Schill H, *et al*. Solid immersion facilitates fluorescence microscopy with nanometer resolution and sub-ångström emitter localization. *Adv Mater*. 2012;24(44):OP309-OP313. doi: 10.1002/adma.201203033.

138. Liaros N, Fourkas JT. Ten years of two-color photolithography. Invited. *Opt Mater Express*. 2019;9(7):3006. doi: 10.1364/ome.9.003006.

139. Fischer J, von Freymann G, Wegener M. The materials challenge in diffraction-unlimited direct-laser-writing optical lithography. *Adv Mater*. 2010;22(32):3578-3582. doi: 10.1002/adma.201000892.

140. Li L, Gattass RR, Gershgoren E, *et al*. Achieving λ/20 resolution by one-color initiation and deactivation of polymerization. *Science*. 2009;324(5929):910-913. doi: 10.1126/science.1168996.

141. He M, Zhang Z, Cao C, *et al*. 3D sub-diffraction printing by multicolor photoinhibition lithography: from optics to chemistry. *Laser Photonics Rev*. 2022;16(2):2100229. doi: 10.1002/lpor.202100229.

142. Fischer J, Ergin T, Wegener M. Three-dimensional polarization-independent visible-frequency carpet invisibility cloak. *Opt Lett*. 2011;36(11):2059-2061. doi: 10.1364/ol.36.002059.

143. Fischer J, Wegener M. Three-dimensional direct laser writing inspired by stimulated-emission-depletion microscopy. Invited. *Opt Mater Express*. 2011;1(4):614-624. doi: 10.1364/OME.1.000614.

144. Wolf TJA, Fischer J, Wegener M, *et al*. Pump-probe spectroscopy on photoinitiators for stimulated-emission-depletion optical lithography. *Opt Lett*. 2011;36(16):3188-3190. doi: 10.1364/OL.36.003188.

145. Wollhofen R, Katzmann J, Hrelescu C, *et al*. 120 nm resolution and 55 nm structure size in STED-lithography. *Opt Express*. 2013;21(9):10831-10840. doi: 10.1364/OE.21.010831.

146. Fischer J, Mueller JB, Quick AS, *et al*. Exploring the mechanisms in STED-enhanced direct laser writing. *Adv. Opt. Mater.* 2015;3(2):221-232. doi: 10.1002/adom.201400413.

147. Zhu D, Xu L, Ding C, *et al*. Direct laser writing breaking diffraction barrier based on two-focus parallel peripheral-photoinhibition lithography. *Adv Photonics*. 2022;4(6):066002. doi: 10.1117/1.AP.4.6.066002.

148. He M, Zhang Z, Cao C, *et al*. Single-color peripheral photoinhibition lithography of nanophotonic structures. *PhotoniX*. 2022;3(1):25. doi: 10.1186/s43074-022-00072-2.

149. Ding C, Liu X, Liu Q, *et al*. Subdiffraction 3D nanolithography by two-photon two-step absorption and photoinhibition. *Laser Photonics Rev*. 2023;18(3):2300645. doi: 10.1002/lpor.202300645.

150. Fischer J, Wegener M. Ultrafast polymerization inhibition by stimulated emission depletion for three-dimensional nanolithography. *Adv Mater*. 2012;24(10):OP65-OP69. doi: 10.1002/adma.201103758.

151. Donnert G, Keller J, Medda R, *et al*. Macromolecular-scale resolution in biological fluorescence microscopy. *Proc Natl Acad Sci*. 2006;103(31):11440-11445. doi: 10.1073/pnas.0604965103.

152. Harke B, Bianchini P, Brandi F, *et al*. Photopolymerization inhibition dynamics for sub-diffraction direct laser writing lithography. *Chemphyschem*. 2012;13(6):1429-1434. doi: 10.1002/cphc.201200006.

153. Harke B, Dallari W, Grancini G, *et al*. Polymerization inhibition by triplet state absorption for nanoscale lithography. *Adv Mater*. 2013;25(6):904-909. doi: 10.1002/adma.201204141.

154. Thiel M, Ott J, Radke A, *et al*. Dip-in depletion optical lithography of three-dimensional chiral polarizers. *Opt Lett*. 2013,38(20):4252-4255. doi: 10.1364/OL.38.004252.

155. Somers P, Liang Z, Chi T, *et al*. Photo-activated polymerization inhibition process in photoinitiator systems for high-throughput 3D nanoprinting. *Nanophotonics*. 2023;12(8):1571-1580. doi: 10.1515/nanoph-2022-0611.

156. Stocker MP, Li L, Gattass RR, *et al*. Multiphoton photoresists giving nanoscale resolution that is inversely dependent on exposure time. *Nat Chem*. 2011;3(3):223-227. doi: 10.1038/nchem.965.

157. Liaros N, Tomova Z, Razo SAG, *et al*. The state of the art in multicolor visible photolithography. *Proceedings Novel Patterning Technologies*. 2018;10584:26-32, doi: 10.1117/12.2297653

158. Mueller P, Zieger MM, Richter B, *et al*. Molecular switch for sub-diffraction laser lithography by photoenol intermediate-state cis-trans isomerization. *ACS Nano*. 2017;11(6):6396-6403. doi: 10.1021/acsnano.7b02820.

159. Müller P, Müller R, Hammer L, *et al*. STED-inspired laser lithography based on photoswitchable spirothiopyran moieties. *Chem Mater*. 2019;31(6):1966-1972. doi: 10.1021/acs.chemmater.8b04696.

160. Andrew TL, Tsai HY, Menon R. Confining light to deep subwavelength dimensions to enable optical nanopatterning. *Science*. 2009;324(5929):917-921. doi: 10.1126/science.1167704.

161. Cao Y, Gan Z, Jia B, *et al*. High-photosensitive resin for super-resolution direct-laser-writing based on photoinhibited polymerization. *Opt Express*. 2011;19(20):19486-19494. doi: 10.1364/OE.19.019486.

162. Gan Z, Cao Y, Evans RA, *et al*. Three-dimensional deep sub-diffraction optical beam lithography with 9 nm feature size. *Nat Commun*. 2013;4(1):2061. doi: 10.1038/ncomms3061.

163. Guan L, Cao C, Liu X, *et al*. Light and matter co-confined multi-photon lithography. *Nat Commun*. 2024;15(1):2387. doi: 10.1038/s41467-024-46743-5.

164. Zvagelsky R, Mayer F, Beutel D, *et al*. Towards in-situ diagnostics of multi-photon 3D laser printing using optical coherence tomography. *Light Adv Manuf*. 2022;3(3):1. doi: 10.37188/lam.2022.039.

165. He Y, Shao Q, Chen S-C, *et al*. Characterization of two-photon photopolymerization fabrication using high-speed optical diffraction tomography. *Addit Manuf*. 2022;60:103293. doi: 10.1016/j.addma.2022.103293.

166. Wang H, Liu S, Yin X, *et al*. Polar-coordinate line-projection light-curing continuous 3D printing for tubular structures. *Int J Extreme Manuf*. 2024;6(4):045004. doi: 10.1088/2631-7990/ad3c7f.

167. Wang H, Gao F, Shi Y, *et al*. Sparse-view irradiation processing volumetric additive manufacturing. *Int J Extreme Manuf*. 2025;7(6):065001. doi: 10.1088/2631-7990/adebbf.

168. Hu N, Ding L, Wang A, *et al*. Comprehensive modeling of corkscrew motion in micro-/nano-robots with general helical structures. *Nat Commun*. 2024;15(1):7399. doi: 10.1038/s41467-024-51518-z

169. Johnson JE, Chen Y, Xu X. Model for polymerization and self-deactivation in two-photon nanolithography. *Opt Express*. 2022;30(15):26824. doi: 10.1364/oe.461969.

170. Pingali R, Saha SK. Reaction-diffusion modeling of photopolymerization during femtosecond projection two-photon lithography. *J Manuf Sci Eng*. 2021;144(2):021011. doi: 10.1115/1.4051830.